NUCLEAR STRUCTURE -- EXPERIMENTAL

THE ELUSIVE PROTON HALO OF ^{8}B STUDIED BY FRAGMENTATION REACTIONS

J. H. Kelley, Sam M. Austin, A. Azhari, D. Bazin, J. A. Brown, M. Fauerbach, M. Hellström, S. E. Hirzebruch, J. J. Kolata[a], R. A. Kryger, K. L. Lamkin[a], D. J. Morrissey, R. Pfaff, C. F. Powell, E. Ramakrishnan, B. M. Sherrill, M. Steiner, T. Suomijarvi, M. Thoennessen and J. S. Winfield.

Recent interest in radioactive nuclear beams has focused mainly on the weakly bound nuclei ^{11}Li and ^{11}Be and the low density neutron halo region that these nuclei possess [1]. The halo, which can be thought of as the valence neutrons orbiting a compact core at an extended distance, is the result of extensive quantum barrier penetration that permits anomalously large core-neutron separation distances [2]. Although the 790A MeV reaction cross section data of Tanihata *et al.* [3] showed clear evidence (large cross sections) of neutron halos there was no evidence for a proton halo in ^{8}B, although it is bound by only 140 keV. It appeared the that additional barrier height provided by the Coulomb potential prevented the valence proton from penetrating deeply outside of the potential well of the ^{7}Be core [4]. However, a measurement of the quadrupole moment of ^{8}B indicated that the valence proton does extend appreciably beyond the ^{7}Be core radius [5]. Furthermore a recent measurement of the reaction cross section of 20-60A MeV ^{8}B in active Si targets also indicated an enhanced radius [6].

To resolve the existing discrepancies we have approached the issue by measuring fragment momentum distributions. In a simple interpretation originally developed by Serber for deuteron breakup [7], the momentum distribution of ^{7}Be core fragments is related to the Fourier transform of the spatial wavefunction of the valence proton. With this interpretation (which neglects reaction mechanism and final state interaction effects) a narrow ^{7}Be fragment momentum distribution width would indicate an extended spatial distribution for the proton. We have simultaneously measured the parallel and transverse momentum distributions ($p_{\|}$ and $p_{\perp}$) of ^{7}Be fragments following the breakup of 41A MeV ^{8}B in Be, Nb and Au targets. The narrow fragment $p_{\|}$ distribution widths that we observe are consistent with the presence of a proton halo, though a dependence of the width on the target mass appears to indicate that in this case reaction mechanism effects play a role in determining the final momentum distribution.

Some of the most convincing evidence for neutron halos has come from measurements of the momentum distribution of halo and core fragments. Although $p_{\perp}$ distribution measurements of halo and core fragments from the breakup of ^{6}He, ^{11}Li and ^{11}Be clearly indicate the presence of extended neutron distributions, $p_{\perp}$ is perturbed by reaction mechanism effects such as diffraction, absorption and Coulomb deflection. The $p_{\|}$ distribution following a direct breakup is less perturbed by these reaction effects [8] and should more accurately reflect the initial state momentum distribution of the fragments in the nucleus prior to the breakup. In earlier letters we have shown that the $p_{\|}$ distributions of ^{9}Li fragments from ^{11}Li [9] and ^{10}Be fragments from ^{11}Be [10] are in good agreement with theoretical predictions.

A radioactive nuclear beam of ^{8}B particles was produced by fragmenting 60A MeV ^{16}O ions, provided by the K1200 cyclotron at the National Superconducting Cyclotron Laboratory, in a thick Be production target. After passing through the A1200 fragment separator, with an Al absorber (wedge) placed at the second dispersive image, the beam consisted of the N=3 isotones. The beam then passed through the RPMS Wien filter which separated the isotones, so that a 95% pure 41.2A MeV ^{8}B beam reached the breakup targets. To insure that the detected ^{7}Be particles came from reactions of ^{8}B in the

target, incoming particles were identified as ^{8}B by their time-of-flight over a 40 meter flight path between a thin plastic scintillator and the particle detector telescopes. The ^{8}B beam momentum spread was limited to 0.5% by an aperture located at the first dispersive image of the A1200. This provided approximately 300 ^{8}B particles per second at the breakup target position.

Two two-dimensional position sensitive Parallel Plate Avalanche Counters (PPACs) placed upstream of the target permitted a reconstruction of the incoming particle trajectories. Breakup products were detected in two 5 cm by 5 cm ΔE-ΔE-E telescopes. The first ΔE detector was a position sensitive Si detector that was segmented into 16 vertical strips and 16 horizontal strips. The second was a Si PIN-diode, and the E signal was provided by a stopping CsI detector. Telescope 1 was 60 cm from the target and covered angles θ=-3.3° to 1.4° (horizontal) and $\phi = \pm 2.4°$ (vertical). The second, Telescope 2, was 50 cm away from the target and covered the angles $\theta = 2.6°$ to 8.3° and $\phi = \pm 2.9°$. An energy calibration was obtained by producing ^{7}Be beams at 6 different energies, using two A1200 magnetic rigidity settings and two beam-energy degraders upstream of the telescopes.

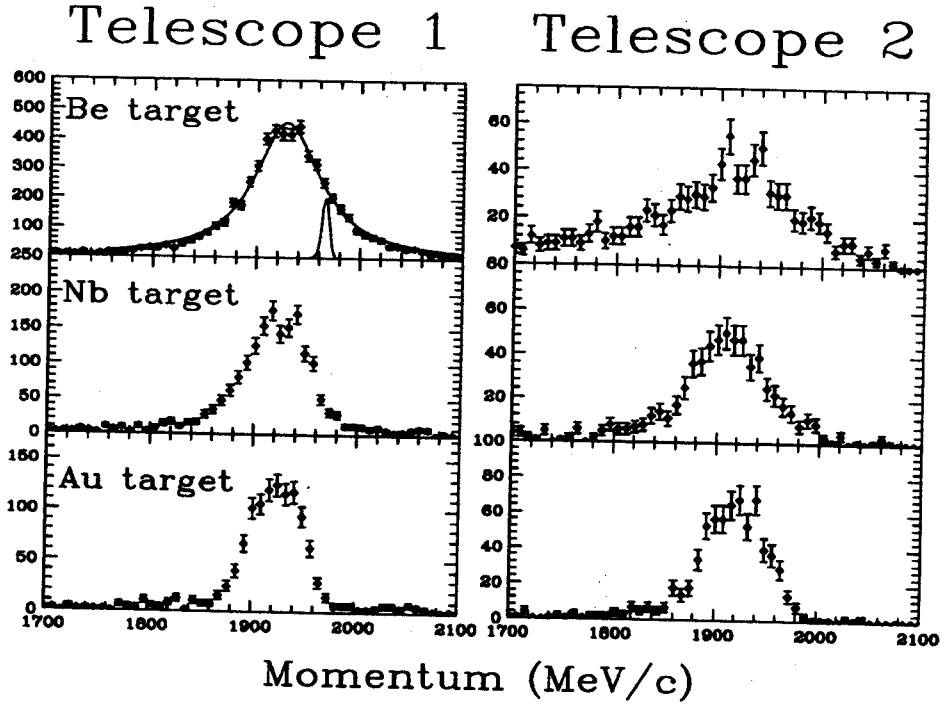

Figure 1: The $p_{\|}$ distributions of ^{7}Be fragments from the breakup of ^{8}B on Be, Nb, and Au targets. Shown on the figure for the Be target is a small narrow peak which illustrates the momentum resolution from one of the energy calibration points. Also shown with the Be data is a Lorentzian fit (Γ=77 MeV/c) to the central 10 % of the distribution. Target out data indicates that the background is small (less than 1 count per bin in the case of the Au target) and relatively flat.

The ^{7}Be fragment $p_{\|}$ distributions measured in Telescope 1 are similar in width for all targets, although slightly narrower for the heavier targets. The Telescope 2 data indicate that the distributions become broader at larger scattering angles with a strong target dependence. A Lorentzian shaped momentum distribution leads to an angular dependence similar to that observed from the Be target, though it appears from the observations on the other targets that the reaction mechanism also plays an active role. We describe the data in Table 1 in terms of the Full Width at Half Maximum in order to avoid

any bias for a particular lineshape.

Target	Uncorrected FWHM (MeV/c)	Resolution and Beam spread (MeV/c)	Differential E-loss ^{7}Be and ^{8}B (MeV/c)	Corrected FWHM (MeV/c)	^{8}B Rest Frame (MeV/c)	Energy at mid target (MeV/A)
Telescope 1						
Be	84	13.5	8	83	79	40.3
Nb	72	13.5	10	70	67	40.0
Au	66	13.5	8	64	62	40.1
Telescope 2						
Be	130	12.1	8	129	124	40.3
Nb	88	12.1	10	87	83	40.0
Au	69	12.1	8	67	65	40.1

Table 1: Summary of the preliminary results of the $p_{||}$ distributions.

The contributions of experimental effects that broaden the observed $p_{||}$ distributions are subtracted, in quadrature, and are detailed in Table 1. The narrow momentum aperture at Image 1 of the A1200 permits only a 0.5% spread in the momentum of the incoming ^{8}B beam. Other corrections are for the momentum resolution of the telescopes (0.5% FWHM after correcting for the position dependent response of the CsI detectors), and the broadening effects associated with the differential energy loss of the ^{7}Be and ^{8}B in the thick reaction targets (47 mg/cm^2 Be, 85 mg/cm^2 Nb, and 97 mg/cm^2 Au). Transformation into the ^{8}B rest frame reduces the width by 4%.

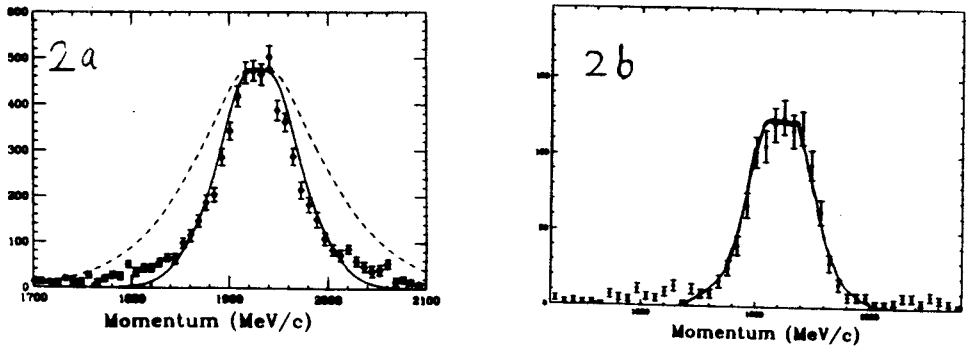

Figure 2: Predictions for the $p_{||}$ distributions for breakup on light and heavy targets. Figure 2a compares data from the Be target with the $p_{||}$ distribution obtained from the Fourier transform of the wavefunction of the valence proton without (solid) and with the absorptive cut-off (dashes) [11]. Figure 2b compares data from the Au target with the $p_{||}$ distribution obtained from a Coulomb dissociation calculation [12] at an impact parameter of 15 fm.

Measurements of the reaction cross section data for neutron halo nuclei and the corresponding theoretical calculations have led to a conclusion that nuclear processes dominate breakups on light targets, while Coulomb processes dominate breakups on heavy targets [13]. We assume this also holds true for ^{8}B The Serber model yields a broad distribution (150 MeV/c FWHM) for a Woods-Saxon potential well that yields the correct binding energy [14], not in good agreement with our results. The shell model calculation indicates an rms radius for the valence proton of 4.60 fm and a total rms radius of ^{8}B of 2.71 fm. Unlike the results for ^{11}Be and ^{11}Li, we must incorporate an absorptive cut-off limit such as is used in the Extended Serber model, developed by Utsunomiya [15]. This model assumes that a critical radius exists. The

constituents of the projectile are separated by a distance such that either the halo nucleon can be absorbed without disturbing the core ($R > R_c$) or an interaction with the target would result in a destruction of the core ($R < R_c$). In the Extended Serber model the predicted fragment momentum distribution is obtained from the Fourier transform of the wavefunction outside the absorptive cut-off radius. If R_c is taken as the radius where the halo proton density and core density are equal then the $p_{\|}$ distribution width is reduced to 96 MeV/c [14] and becomes comparable with the data.

Esbensen [12] is developing a model to explain the ^{7}Be fragment momentum distributions in a similar manner as [16], who describe a treatment for stripping, diffraction and Coulomb dissociation. Esbensen specifically considers the behavior of the m_ℓ sub-states of the p-state valence proton in ^{8}B. Because stripping reactions of m_ℓ=0 protons will generally also lead to absorption of the core (since the m_ℓ=0 sub-state is oriented along the beam trajectory), only the $m_\ell = \pm 1$ contributions are considered in stripping reactions. With this assumption he finds that his predicted $p_{\|}$ distributions are reduced from 160 MeV/c, when the full wavefunction is considered, to values near 100 MeV/c.

The ^{7}Be fragment $p_{\|}$ distribution from the Au target is well described by a soft-dipole excitation as in [17], see Fig. 2. The distribution width becomes narrower than for the Be target; it appears that the Coulomb dissociation mechanism yields a smaller width. At higher energies (1471A MeV) the measured $p_{\|}$ distribution widths are the same for both heavy and light targets [18]. This perhaps indicates that the shape of the virtual photon spectrum, which is flatter at higher energies, influences the shape of the ^{7}Be fragment momentum distribution at an energy of 41A MeV. The participation of the first excited state of ^{8}B in the breakup is negligible since a complete kinematics measurement of the Coulomb dissociation of ^{8}B [19] indicates that the reaction is dominated by breakup into continuum states.

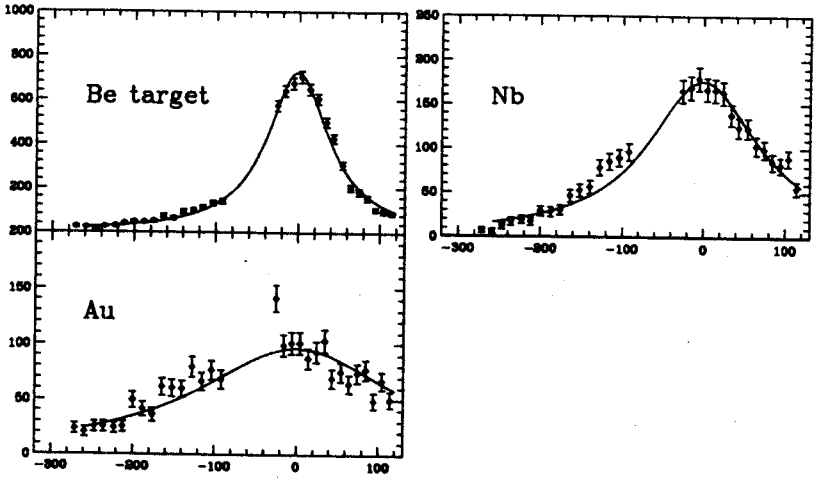

Figure 3: The p_x distributions of ^{7}Be fragments from the breakup of ^{8}B.

The $p_\perp$ distributions do not reveal the proton halo as clearly as the $p_{\|}$ distributions do. We consider the p_x distribution which is a projection of $p_\perp$ onto one axis. The width of the p_x distribution from breakup on the Be target is in good agreement with the $p_{\|}$ distributions after making small corrections for the angular spread of the incoming beam, multiple scattering and a small Coulomb deflection (defined as the grazing angle). However the results for breakup on the heavier targets are much broader, in a manner that cannot be interpreted in a simple model. It is likely that Coulomb deflection plays a considerable role

in determining these widths.

Target	Uncorrected FWHM (MeV/c)	Resolution and Beam spread (MeV/c)	Multiple scattering (MeV/c)	Corrected FWHM (MeV/c)
Be	92	26	8	88
Nb	166	26	34	160
Au	298	26	56	291

Table 2: Summary of preliminary results for the p_x distributions.

In conclusion, we find that the ^{7}Be fragment $p_{\|}$ distributions are narrow and indicate that the valence proton extends significantly beyond the core radius. The $p_{\perp}$ distributions are clearly influenced by reaction effects, thus we focus our attention on the $p_{\|}$ distributions. An absorptive cut-off radius is necessary to reproduce the observed width on the Be target, which could be due to the fact that the proton halo of ^{8}B does not extend as far away from the core as the neutron halos of ^{11}Li and ^{11}Be. Because the width of the $p_{\|}$ distributions decrease with increasing target mass, it appears that the reaction mechanism does influence the measured distributions in this case.

a. Department of Physics, University of Notre Dame, Notre Dame,IN 46556

References

1. A.C. Mueller and B.M. Sherrill, Annu. Rev. Nucl. Part. Sci. 43, 529 (1993).
2. P.G. Hansen and B. Jonson, Europhys. Lett., 4, 409 (1987).
3. I. Tanihata *et al.*, Phys. Lett. B 206, 592 (1988).
4. P.G. Hansen, Nucl. Phys. A553, 89c (1993).
5. T. Minamisono *et al.*, Phys. Rev. Lett. 69, 2058 (1992).
6. R. E. Warner *et al.*, submitted to Phys. Rev. C.
7. R. Serber, Phys. Rev. 72, 1008 (1947).
8. C.A. Bertulani and K.W. McVoy, Phys. Rev. C 46, 2638 (1992).
9. N.A. Orr *et al.*, Phys. Rev. Lett. 69, 2050 (1992).
10. J.H. Kelley *et al.*, Phys. Rev. Lett. 74, 30 (1995).
11. B.A. Brown private communication.
12. H. Esbensen private communication.
13. R. Anne *et al.*, Phys. Lett. B 304, 55 (1993).
14. B.A. Brown, A. Csoto, and R. Sherr, submitted to Nucl. Phys. A.
15. Utsunomiya, Phys. Rev. C 32, 849 (1985).
16. F. Barranco, E. Vigezzi and R.A. Broglia, Phys. Lett. B 319, 387 (1993).
17. H. Esbensen and G.F. Bertsch, Nucl. Phys. A542, 310 (1992).
18. W. Schwab *et al.*, Z. Phys. A 350, 283 (1995).
19. T. Motobayashi *et al.*, Phys. Rev. Lett. 73, 2680 (1994).

THE ONE-NEUTRON HALO OF ^{19}C

D. Bazin, B.A. Brown, J. Brown, M. Fauerbach, M. Hellström,
S.E. Hirzebruch, J.H. Kelley, R.A. Kryger, D.J. Morrissey, R. Pfaff, C.F. Powell,
B.M. Sherrill and M. Thoennessen

Nuclear halos are a new form of nuclear matter which appears in loosely bound systems where the valence wave function extends far beyond the standard size. Nuclei with this property have recently triggered great interest both experimentally and theoretically [1]. The formation of halos originates from the tunneling of one or a few valence nucleon(s) outside the potential, but unlike other kind of tunneling such as α-decay, the nucleon(s) remain bound to the nucleus.

The only case of a one-neutron halo known so far is in ^{11}Be, which has been extensively studied [2-3-4] and provides a critical test of halo theories since its shell structure is well understood, and its halo consists of a single neutron. Here we report the observation of a new example of a one-neutron halo in the nucleus ^{19}C [5]. It is the heaviest halo nucleus observed so far, and its study will allow us to further explore the characteristics of the halo phenomenon, in particular in testing the arguments and concepts developed for ^{11}Be.

The nucleus ^{19}C is the last bound odd-neutron isotope of carbon. Its mass has been determined using Time-of-Flight techniques from which a weighted average yields a one-neutron separation energy of S_n= 242 ± 95 keV. This value is significantly lower than the separation energy of ^{11}Be (504 ± 6 keV) which indicates that the halo of ^{19}C should be larger. From a simple filling of the orbitals, the last neutron of ^{19}C should be in the $0d_{5/2}$ orbit, where the ℓ=2 centrifugal barrier would strongly limit the extent of the halo, as shown by recent calculations [6]. However, recent shell-model calculations based on the Warburton-Brown effective interaction [7] actually predict an s-state for the ^{19}C ground state, due to the lowering of the $1s_{1/2}$-orbit [5]. Although the ground state of ^{19}C is not known experimentally, it is interesting to note that the intrusion of an s-state as the ground state would be very similar to the case of ^{11}Be, for which the same effective interaction correctly predicts the $J^\pi = \frac{1}{2}^+$ s ground state [8].

One of the most direct methods to measure the size of a halo nucleus is by removing the loosely bound particle(s) in a breakup reaction and measuring the momentum of the outgoing fragments. The reaction can result from either Coulomb or nuclear dissociation. Although both reaction channels always coexist, the Coulomb dissociation cross section dominates for heavy targets, whereas it becomes negligible for light targets where the nuclear dissociation cross section is predominant. According to the complementarity principle, the width of the internal momentum distribution of the loosely bound particle(s) is inversely proportionnal to the spacial extent of the halo. Measurements of the longitudinal momentum distribution of the core after breakup have been successfully used to measure the size of halos in the nuclei ^{11}Li [9] and ^{11}Be [4]. In this experiment, we have measured the longitudinal momentum of the ^{18}C core after the one neutron breakup of ^{19}C on a Be target.

^{19}C was produced from the fragmentation of a 90 MeV/A ^{40}Ar beam on a 470 mg/cm^2 thick Be target. The observed yield was of 0.36 nuclei per second for an average primary beam intensity of (26) pnA. The secondary beam was transported through the A1200 magnetic spectrometer [10] up to its second image dispersive plane, where the breakup reaction target was placed. The reaction products were then analysed in momentum by the last section of the A1200 where the rigidity was set on the central momentum of the ^{18}C ions coming from the breakup reaction.

Although the secondary beam had a large energy spread due to the fragmentation process, large enough to fill the momentum acceptance of the spectrometer (3%), it was still possible to achieve a resolution of 0.12% using a dispersion-matched mode [11] in which the momentum dispersion caused

by the first section of the A1200 is compensated by the last section. The horizontal position of the particles arriving at the final focal plane was measured using a position-sensitive silicon detector (PSD) which also provided the energy loss measurement. The residual energy was measured in a thick plastic scintillator stop detector located behind the PSD. The Time-of-Flight (TOF) from the ^{19}C production target to the final focal plane was measured between the stop detector and the rf cyclotron signal. The momentum calibration was determined by stepping the rigidity of the last section and measure the position of ions of known rigidity at the final focal plane.

The particle identification was calibrated using the numerous contaminants transmitted along with the ^{19}C beam. A complication arised from the fact that a reaction occurs within the spectrometer where a nucleus $^{A_1}Z_1$ is transformed into $^{A_2}Z_2$. A double identification can be made using the following method : the $^{A_2}Z_2$ particle is identified using the energy loss ΔE, the total kinetic energy, TKE, and the magnetic rigidity of the last section $B\rho_3 = B\rho_3^0 + D_3 \times x_3$ measured at the final focal plane. From the usual relativistic equations, one can extract the relativistic parameter of the particle after the reaction : $\gamma_2 = B/(B-1)$ where $B = \frac{B\rho_3}{3.107}\frac{c^2}{TKE}k\sqrt{\Delta E}$ and k is a constant. The full identification of this particle follows simply. Its time-of-flight $TOF2$ from the breakup target to the final focal plane can then be determined and substracted to the total time-of-flight to obtain $TOF1$=TOF-$TOF2$. This allows one to measure the A/Z ratio of the particle before the reaction using the relation $B\rho_1 = 3.107\beta_1\gamma_1 A_1/Z_1$. Fig. 1 shows a plot of $A2$ versus $A1/Z1$ for $Z2$>3. The group of events corresponding to the one neutron breakup of ^{19}C is clearly identified, but there are in addition two other groups which can be attributed to the one neutron breakup of ^{18}C and ^{17}C which were transmitted as contaminants. The longitudinal momentum distributions observed for the 3 reactions mentioned above are presented in Fig. 2. The striking difference between the width of ^{19}C and that of its neighbours ^{18}C and ^{17}C is a clear indication of the halo structure of ^{19}C.

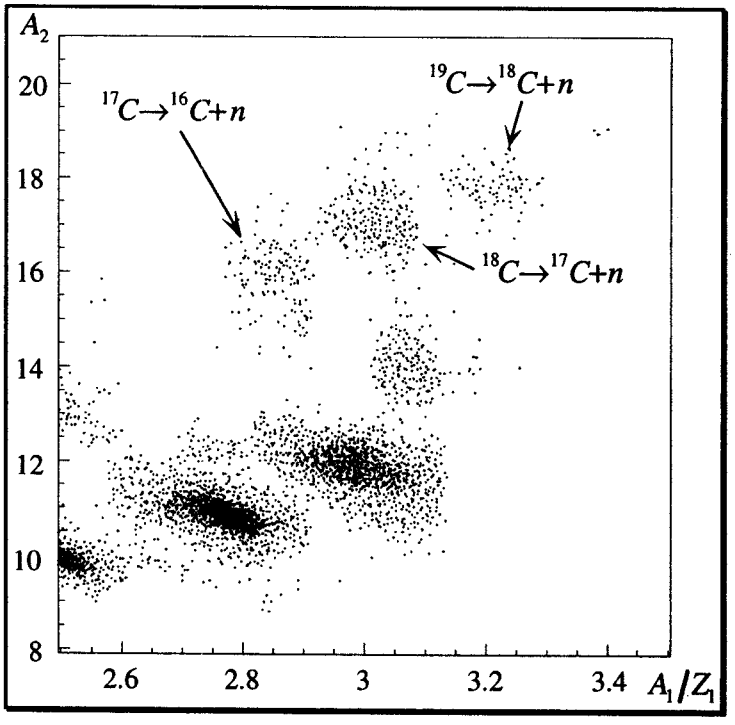

Figure 1: Plot of the mass A_2 of the particles after the breakup target as a function of the A_1/Z_1 ratio of the particles before.

Assuming that the last neutron is in an s orbit, the external wave function can be modeled as an exponential decay (Yukawa) of the form $\exp(-r/\rho)/r$ where the decay length $\rho = \hbar/\sqrt{2\mu S_n}$ is expressed in terms of the reduced mass μ and the one-neutron separation energy S_n. The Fourier transform of this wave function has a Lorentzian shape $\left|\tilde{\Psi}(\vec{p})\right|^2 \equiv \frac{d\vec{p}}{\left(\hbar^2/\rho^2 + \vec{p}^2\right)^2}$ of width Γ related to the decay length by $\Gamma = 2\hbar/\rho = 2\sqrt{2\mu S_n}$. The r.m.s. radius of the halo is then given by

$\langle r^2 \rangle^{1/2} = \rho/\sqrt{2}$. As pointed out in [4], the acceptances $\Delta\theta$ and $\Delta\phi$ of the spectrometer change the shape of the Lorentzian momentum distribution. The analytical form of this shape can be easily calculated [5]. For the acceptances of the A1200 at our energy, the change in width of the distribution is of the order of 5-10%. In addition to the determination of the FWHM of the distributions, we have used this analytical form to fit our data and extract the width Γ. All experimental results and the quantities derived from them are summarized in Table 1. The separation energies for ^{17}C and ^{18}C are extracted from Audi et al. [12].

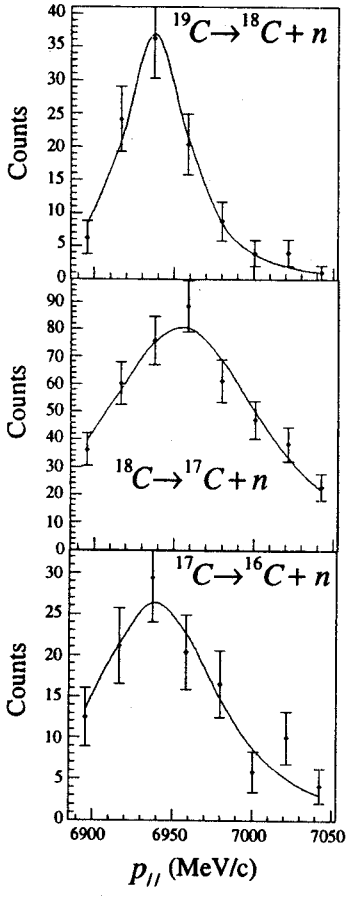

Figure 2: Longitudinal momentum distributions of the recoiling fragment in the one-neutron breakup of ^{19}C, ^{18}C and ^{17}C.

A comparison between the r.m.s. radii deduced for ^{19}C and ^{17}C and the radii of the ^{18}C and ^{16}C cores calculated from the constant density law $R = r_0 A^{1/3}$ with r_0 = 1.12 fm (2.93 fm and 2.82 fm respectively) shows that the halo of ^{19}C extends far beyond the ^{18}C core, whereas the r.m.s. radius of the last neutron of ^{17}C is of the same order as the size of the ^{16}C core. The one-neutron breakup cross-section follows the same trend, as it is significantly larger for ^{19}C than for ^{17}C. This difference should be even more pronounced in the Coulomb dissociation cross-sections, which will be soon measured in an upcoming experiment. The last column of Table 1 displays the width Γ as calculated from the separation energy. This width is compatible within error bars with the value we deduce from our fit for the ^{19}C data, but is somewhat small in comparison with the ^{17}C data.

In summary, we have simultaneously measured the longitudinal momentum distributions of ^{18}C, ^{17}C and ^{16}C following the breakup of ^{19}C, ^{18}C and ^{17}C. In the ^{19}C data, both the observation of a narrow momentum peak and a large cross-section indicate the presence of a one-neutron halo. This conclusion coincides with a shell-model calculation which predicts an s-state for the ^{19}C ground state. The ^{17}C data also show a narrow momentum peak, but it is wider and therefore incompatible with the width deduced from the binding energy in the assumption of a s-state neutron halo. Hence ^{17}C may be the first observed case of a "hindered halo" due to the presence of a ℓ=2 centrifugal barrier. Indeed, the shell-model calculation mentioned above predicts a d-state for the ^{17}C ground state, in agreement with this conclusion. More complete data would be most welcome, in particular on the mass of ^{19}C, but also on the one-neutron Coulomb dissociation of ^{17}C and ^{19}C.

Carbon Isotope	Energy (MeV/u)	FWHM MeV/c	Γ (MeV/c)	$\langle r^2 \rangle$ (fm)	σ_{1n} (mb)	S_n (keV)	Γ from S_n (MeV/c)
19	79.6	44.3 ± 5.9	50.8 ± 8.8	5.5 ± 0.9	105 ± 17	242 ± 95	41 ± 12
18	88.3	110.3 ± 12.4			34.8 ± 2.1	4180 ± 30	
17	98.5	82.5 ± 15.9	104 ± 19	2.7 ± 0.6	40.9 ± 4.3	729 ± 18	71.5 ± 0.9

Table 1 : Summary of experimental results and deduced quantities.

References

1. P.G. Hansen, Nucl. Phys. A **553**, 89c (1993) and references therein.
2. M. Fukuda et al., Phys.Lett. B **268**, 339 (1991)
3. R. Anne et al., Phys. Lett. B **304**, 55 (1993).
4. J. Kelley et al., Phys. Rev. Lett. **74**, 30 (1995)
5. D. Bazin et al., Phys. Rev. Lett. **74**, 3569 (1995)
6. K. Riisager, A.S. Jensen, P. Møller, Nucl.Phys. A **548**, 393 (1992).
7. E.K. Warburton, B.A. Brown, Phys. Rev. C **46**, 923 (1992).
8. H. Sagawa, B.A. Brown, H. Esbensen, Phys. Lett. B **309**, 1 (1993).
9. N. Orr et al., Phys. Rev. Lett. **69**, 2050 (1992).
10. B.M. Sherrill et al., Nucl. Instrum. and Meth. B **56/57**, 1106 (1991).
11. B.L. Cohen, Rev. Sci. Instrum. **30**, 415 (1959).
12. G. Audi, A.H. Wapstra, Nucl. Phys. A **565**, 1 (1993).

FIRST STUDY OF HEAVY–ION MIRROR CHARGE EXCHANGE

M. Steiner, Sam M. Austin, D. Bazin, W.A. Benenson, C.A. Bertulani[a], J.A. Brown, M. Fauerbach, M. Hellström[b], E. Kashy, J.H. Kelley, R.A. Kryger, T. Kubo[c], D.J. Morrissey, N.A. Orr[d], R. Pfaff, C.F. Powell, B.M. Sherrill, M. Thoennessen, S.J. Yennello[e], B.M. Young[f], P.D. Zecher

Among the new capabilities provided by radioactive nuclear beams are nuclear reaction studies with mirror nuclei, since only one member of a mirror pair can be stable. Due to their special symmetry, mirror pairs are a useful tool for the study of the strong force in a nuclear environment, and this provides a unique opportunity for attaining the long–term goal of understanding charge exchange in heavy ions. In the present work, we study the relative importance of spin–flip and non–spin–flip contributions to heavy–ion charge exchange (HICEX) and investigate the usefulness of the reaction for determining Gamow–Teller (GT) transition strengths in nuclei.

The most direct measurements of GT transition strengths, B(GT), are obtained from allowed β–decay, but are limited by the small accessible energy range. Charge–exchange (p,n) reactions at energies above 200 MeV have long been used to measure GT strengths over a wide range of excitation energies, and a well–established relationship exists between the forward cross section $d\sigma/d\Omega(0°)$ and B(GT) [1,2]. This latter method can in principle also be used for unstable nuclei by means of inverse–kinematics experiments with radioactive beams on hydrogen targets. If good energy resolution is to be obtained, however, these experiments will be difficult, since they involve the detection of rather low energy neutrons, and experiments in the β^+ direction are not possible, as there are no neutron targets.

Heavy–ion charge exchange has the potential to become a powerful tool for GT strength measurements if a reliable calibration analogous to the (p,n) reaction can be found or, more desirably, if the reaction mechanism and its relation to GT strength can be understood in detail. HICEX offers favorable kinematics, the capability to sample both the β^+ and β^- directions, and the additional advantage of quantum selectivity for certain projectile–ejectile choices. In the (^{6}Li,^{6}He) reaction, for example, final states can be chosen which limit the transitions to $\Delta S = 1, \Delta T = 1$ [3].

Two ^{13}C(^{13}N,^{13}C)^{13}N experiments were performed with secondary–beam energies per nucleon of 57 and 105 MeV. The A1200 fragment separator was used in a dispersion–matched mode [4], achieving an energy resolution (FWHM) of 1 MeV (1.5 MeV) at E/A = 57 MeV (105 MeV) despite an energy spread of the secondary beam of about 15 MeV (27 MeV). Detailed experimental parameters are given in Table . The primary ^{14}N beam impinged on a thick ^{9}Be target, producing projectile fragments with near–beam velocity. The first A1200 dipole stage was set to select ^{13}N ions and focus them on a thin ^{13}C–labeled polyethylene target located at a dispersive intermediate image. The ^{13}C reaction products were focused by the second dipole stage onto the A1200 focal plane, which consisted of two two–dimensional position–sensitive drift chambers, a position–sensitive silicon detector, and a large plastic scintillator. Positions and angles as well as time–of–flight, energy loss, and total–energy signals were recorded for each ion. Particle trajectories measured at the focal plane were converted into scattering angles at the reaction target, and angular distributions were obtained for the secondary beam as well as the reaction products. Using ^{13}N as a test beam, trajectories at the reaction target and the focal plane were recorded simultaneously, and the ion–optical parameters of the A1200 were determined. The excitation energy was measured by means of the momentum dispersion of the ^{13}C nuclei at the focal plane. Those ^{13}N ions which left the reaction target in the 6+ charge state had magnetic rigidities very close to the ^{13}C reaction products and were used

to calibrate the energy scale. The $^{13}N^{6+}/^{13}N^{7+}$ charge state ratio at the two energies was experimentally determined (see Table 1), and the $^{13}N^{6+}$ rate was used to measure secondary–beam intensity.

Fig. 1 shows the focal–plane position spectra recorded simultaneously for the $^{13}N^{6+}$ charge state and the (^{13}N,^{13}C) reaction products at E/A=57 MeV and 105 MeV, respectively. The slight shift and larger width of the ^{13}C g.s. peak compared to $^{13}N^{6+}$ is due to the difference in energy loss in the reaction target.

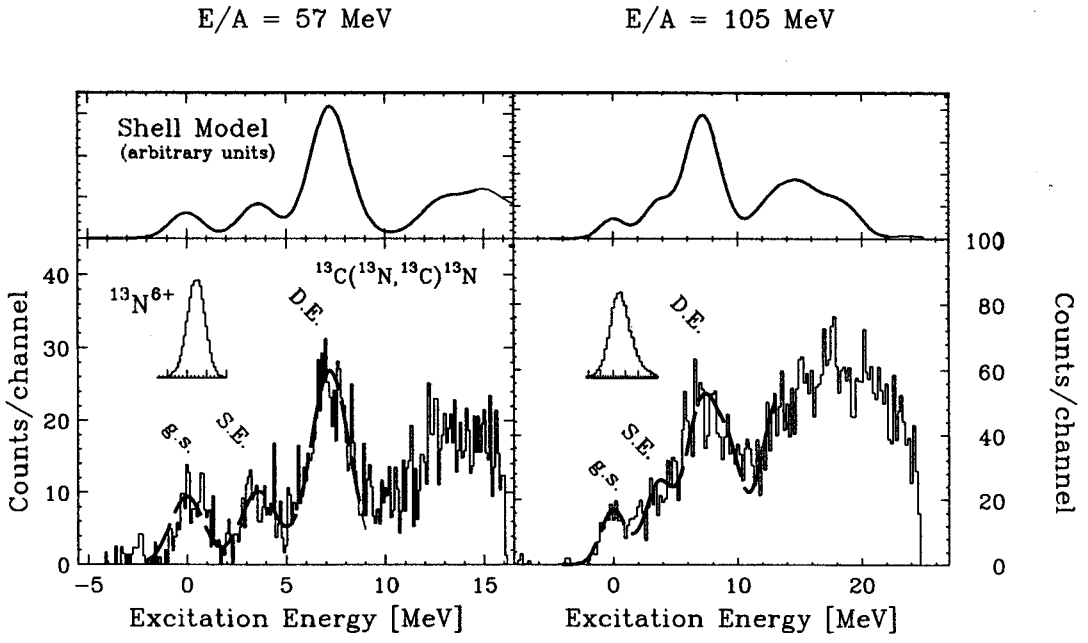

Figure 1: $^{13}C(^{13}N,^{13}C)^{13}N$ energy spectra at energies per nucleon of 57 and 105 MeV. The top curves are calculations using the experimentally obtained unit cross sections per weak–interaction strength and shell–model B(GT) values [8]. The latter are scaled by the conventional quenching factor of 0.67 and the peaks are convoluted with the experimental resolution. The curves closely resemble the general shape of the experimental data (bottom) over the accessible exitation–energy range. The dashed curves are fits to the data with the peak heights as free parameters and are used in determining the cross sections. The insets show the $^{13}N^{6+}$ secondary–beam charge state, observed simultaneously. These indicate the energy resolution achieved with the A1200 fragment separator despite energy spreads of the secondary beams of around 20 MeV.

While peaks in (p,n) spectra can be readily associated with states in the target nucleus, the present situation is complicated by the fact that both target and projectile can be excited. In the following discussion, we will concentrate on the two lowest–lying negative–parity states in the A=13 mirror pair: The $J^\pi=1/2^-$ ground state and the $3/2^-$ excited state at 3.68 MeV (3.50 MeV for ^{13}N). These are the only states below 10 MeV to be strongly excited by charge–exchange reactions in this energy region [5], and they dominate the low–energy part of the spectrum. The peaks marked in Fig. 1 are identified as a) Ground state (g.s.): Both ejectile and target residue are in their ground states, b) Single Excitation (S.E.): The target residue is in the $1/2^-$ ground state and the ejectile in the $3/2^-$ excited state, or vice versa; c) Double Excitation (D.E.): Both nuclei are in their $3/2^-$ excited state. The unresolved structure above 10 MeV excitation energy represents GT transitions to a number of negative–parity states in the 10–to–15 MeV region in the target residue, in combination with GT transitions to either the $1/2^-$ or the $3/2^-$ states in the ejectile as the only particle–stable negative–parity states in ^{13}C.

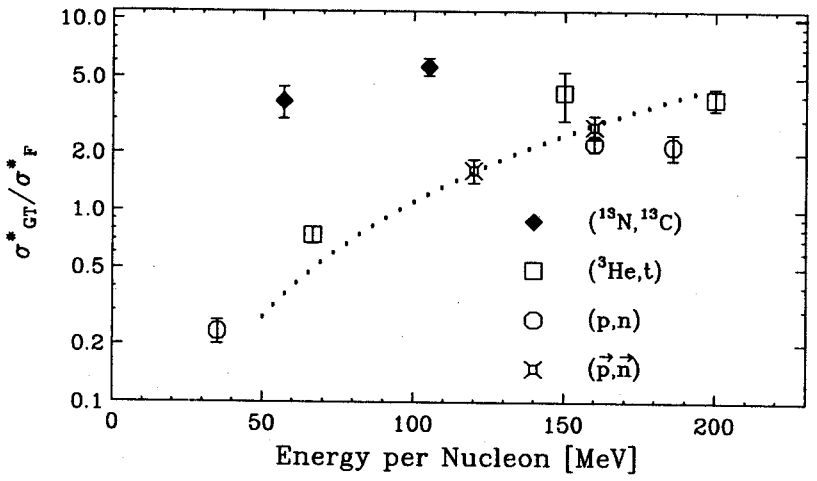

Figure 2: Energy dependence of σ^*_{GT}/σ^*_F for a number of charge–exchange reactions performed on ^{13}C targets. The dotted line is the equivalent of the $\hat{\sigma}_{GT}/\hat{\sigma}_F = (E_p/55\,MeV)^2$ curve, scaled appropriately.

In the (p,n) case, the relationship of zero–degree cross section to target transition strength is conventionally written as

$$d\sigma/d\Omega(0^\circ) = \hat{\sigma}_F F(q,\omega)B(F) + \hat{\sigma}_{GT}F(q,\omega)B(GT), \quad (1)$$

where $\hat{\sigma}_F$ and $\hat{\sigma}_{GT}$ are the cross sections per unit transition strength [2], and F(q, ω) is a function of momentum transfer, q, and energy loss, ω, which approaches unity as q and ω approach zero. F(q, ω) is estimated from systematics [2] to be greater than 0.95 (0.98) for the 57 MeV (105 MeV) experiment and will not be considered in the following. There is an empirical relationship for the ratio of the unit cross sections, which is used in calibrating (p,n) spectra at energies between 50 and 100 MeV: $\hat{\sigma}_{GT}/\hat{\sigma}_F$=$(E_p/55\,MeV)^2$ [2]. For the HICEX case, one needs a more general form for the relationship between cross section and transition strength:

$$d\sigma/d\Omega(0^\circ) = \sigma^*_F B(F)_P B(F)_T + \sigma^*_{GT} B(GT)_P B(GT)_T, \quad (2)$$

where the transition strengths in both projectile (P) and target (T) are taken into account explicitly, and σ^* replaces $\hat{\sigma}$, which is only defined for the (p,n) reaction. The structural similarity of the mirror nuclei

Table 1: Experimental parameters and results for the mirror charge–exchange experiments

^{13}N Energy	E/A=57 MeV	E/A=105 MeV
Intensity (approx.)	5×10^6s^{-1}	6×10^5s^{-1}
Reaction Target	^{13}C, 9.0 mg/cm^2	^{13}C, 18.0 mg/cm^2
^{13}C Resolution	2.0 MeV	2.4 MeV
^{13}N^{6+}/^{13}N^{7+} Ratio	$(1.0\pm0.1)\times10^{-5}$	$(1.5\pm0.2)\times10^{-6}$
$^{13}C_{g.s.}$ $d\sigma/d\Omega(0^\circ)$	17 ±3 mb/sr	16 ±3 mb/sr
$^{13}C_{S.E.}$ $d\sigma/d\Omega(0^\circ)$	15 ±3 mb/sr	22 ±4 mb/sr
$^{13}C_{D.E.}$ $d\sigma/d\Omega(0^\circ)$	44 ±8 mb/sr	56 ±10 mb/sr
σ^*_F	15 ±2 mb/sr	13 ±2 mb/sr
σ^*_{GT}	55 ±10 mb/sr	74 ±13 mb/sr

allows us to write:

$$d\sigma/d\Omega(0°)_{g.s.} = \sigma_F^* B(F)_{1/2^-}^2 + \sigma_{GT}^* B(GT)_{1/2^-}^2 \quad (3)$$

$$d\sigma/d\Omega(0°)_{S.E.} = 2\sigma_{GT}^* B(GT)_{1/2^-} B(GT)_{3/2^-} \quad (4)$$

$$d\sigma/d\Omega(0°)_{D.E.} = \sigma_{GT}^* B(GT)_{3/2^-}^2. \quad (5)$$

There is no mixing of Fermi and GT–type transitions, since the interaction is one–step in nature. Using our measured cross sections, $B(F)_{1/2^-} = 1$, and the literature values $B(GT)_{1/2^-} = 0.200 \pm 0.004$ (β–decay) and $B(GT)_{3/2^-} = 0.83 \pm 0.03$ [5], we can solve for σ_F^* and σ_{GT}^*. The results are given in Table 1. For comparison, we have included experimental results obtained for ^{13}C targets with beams of protons and ^3He [5,6]. The specific cross sections found for the HICEX case are surprisingly large. A test of proportionality that is independent of calibration is obtained by combining Eqs. (4) and (5):

$$\frac{d\sigma/d\Omega(0°)_{D.E.}}{d\sigma/d\Omega(0°)_{S.E.}} = \frac{B(GT)_{3/2^-}}{2\,B(GT)_{1/2^-}}. \quad (6)$$

The experimentally obtained values for the left–hand side of Eq. (6) are 2.2 ± 0.5 (2.3 ± 0.7) for the 57 MeV (105 MeV) experiments, in agreement with the right–hand–side value of 2.08 ± 0.09. For the purpose of comparison, we consider σ_{GT}^*/σ_F^* as a function of energy for the three charge–exchange reactions $^{13}C(p,n)^{13}N$ [5,2], $^{13}C(^3He,t)^{13}N$ [6,7], and $^{13}C(^{13}N,^{13}C)^{13}N$. The result of this analysis is shown in Fig. 2. The data indicate that σ_{GT}^*/σ_F^* increases with projectile mass. We attribute this increase to the strong absorption in heavy–ion reactions, which favors the long–range portion of the nuclear force. The spin–flip part of the interaction is mediated by single–pion exchange and hence is enhanced with respect to the non–spin–flip portion, which has the shorter–range characteristics of multiple–pion exchange.

In conclusion, we have measured the 0° cross sections for the three lowest excitations of the $^{13}C(^{13}N,^{13}C)^{13}N$ reaction in the first mirror charge–exchange experiment. The structure of the excitation spectrum permits a simple interpretation in terms of weak–interaction strengths, and the symmetry of the mirror pair was exploited to determine the cross sections per unit transition strength. The present results are encouraging and indicate that HICEX could become a powerful tool for measurements of GT strengths in radioactive nuclei.

a. Inst. de Fisica, Univ. Federal do Rio de Janeiro, C. Postal 68528, 21945-970 Rio de Janeiro, RJ, Brazil.
b. GSI, Postfach 110552; D–64220 Darmstadt, Germany
c. Cyclotron Laboratory, RIKEN, 2-1 Hirosawa, Wako, Saitama 351-01, Japan.
d. LPC, IN2P3-CNRS, ISMRA et Université de Caen, 14050 Caen Cedex, France.
e. Cyclotron Institute, Texas A&M University, College Station, TX 77843.
f. Department of Physics, Yale University, New Haven, CT 06511.

References

1. C.D. Goodman *et al.*, Phys. Rev. Lett. 44, 1755 (1980).
2. T.N. Taddeucci *et al.*, Nucl. Phys. A469, 125 (1987). Phys. Rev. C 45, 2854 (1992)
3. N. Anantaraman *et al.*, Phys. Rev. C 44, 398 (1991).
4. B.M. Sherrill *et al.*,Nucl. Instr. Methods B56, 1106 (1991).
5. J. Rapaport *et al.*, Phys. Rev. C 36, 500 (1987).
6. J. Jänecke *et al.*, Nucl. Phys. A569, 234c (1994).
7. H. Akimune *et al.*, Nucl. Phys. A569, 234c (1994).
8. W.–T. Chou, B.A. Brown, E.K. Warburton, Phys. Rev. C 47,163 (1993).

A NEW SEARCH FOR ^{26}O

M. Fauerbach, M. Hellström, W. Benenson, R.A. Kryger, J.H. Kelley,
D.J. Morrissey, R. Pfaff, C.F. Powell, and B.M. Sherrill.

An attempt was made to find the very neutron-rich isotope ^{26}O among the fragmentation products of a 90 MeV/nucleon ^{40}Ar beam. This isotope has been predicted to be bound, but was not observed in a previous experiment [1]. As part of the search, the momentum distributions of all the oxygen isotopes in the range from ^{17}O to ^{24}O were carefully determined so that the optimum separator setting for ^{26}O could be used. From an extrapolation of the counting rate of the lighter oxygen isotopes we expected to observe several hundred events of ^{26}O during the measurement. However, no events could be attributed to ^{26}O, thus indicating the particle instability of this isotope. The results for the production cross sections of 72 neutron-rich isotopes, ranging from ^{38}P to ^{11}B, are presented and compared to predictions.

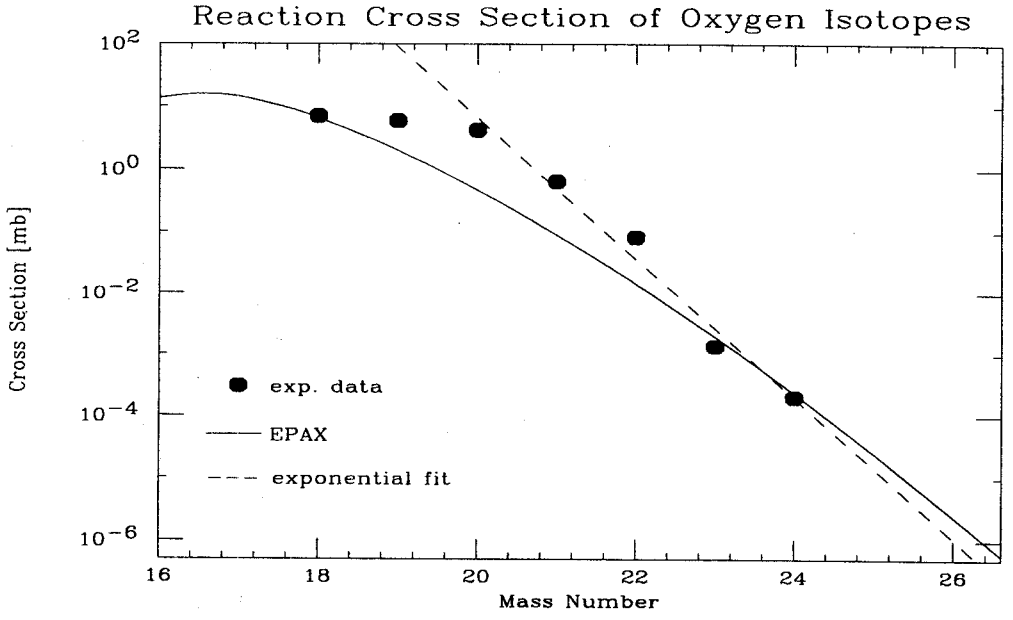

Figure 1: Measured reaction sections for several oxygen isotopes (solid points), ranging from ^{18}O to ^{24}O. The full line indicates the predictions of the semi-empirical formula EPAX [4], and the dashed line is an exponential fit to the experimental data. The extrapolated production cross sections for ^{26}O agree within a factor of two

A 90 MeV/nucleon ^{40}Ar beam from the K1200 cyclotron at the National Superconducting Cyclotron Laboratory at Michigan State University, irradiated a 190mg/cm^2 ^{9}Be target located at the medium acceptance target position of the A1200 fragment separator [2]. The momentum acceptance of the A1200 was ± 1.5% and the angular acceptances were ±10 mrad in θ and ±20 mrad in ϕ. The experimental setup and analysis procedures used for this experiment were similar to those described in Ref. 3. Once the optimum separator setting for ^{26}O was determined, large effort was put into assuring that ^{26}O would be centered at both the intermediate and final focus of the A1200. This was done online by monitoring the ^{19,20}C rates as these particles span ^{26}O in A/Q, namely. During 36 hours at the optimum setting, 2132 events were identified as ^{24}O -approximately an order of magnitude more than the previous

experiment- without a single event that could be attributed to ^{26}O. Fig. 1 shows the measured cross sections for the different oxygen isotopes (solid circles) and the predictions of the semi-empirical formula EPAX [4] (solid line). As can be seen the experimental data and the prediction have a slightly different slope, and therefore a simple exponential fit (dashed line) to the most neutron-rich oxygen isotopes was also used to predict the cross section of ^{26}O. From these extrapolations, we predict a cross section for ^{26}O of 2.43 nb (EPAX) and 1.07 nb (exp. fit). Using these estimates, we should have observed between 400 and 800 counts of ^{26}O respectively. At a 90% confidence level we calculate the upper limit on the ^{26}O production cross section to be 7pb.

References

1. D. Guillemaud-Mueller, et al., Phys. Rev. **C41** (1990) 937.
2. B.M. Sherrill et al., Nucl. Instr. Methods **B56** (1991) 1106.
3. R. Pfaff et al., Phys Rev. **C51** (1995) 1348.
4. K. Sümmerer et al., Phys. Rev **C42** (1992) 2546.

PRODUCTION CROSS SECTIONS OF NEUTRON-RICH ISOTOPES FROM THE FRAGMENTATION OF ^{48}CA AT 100 MEV/NUCLEON

M. Fauerbach, M. Hellström, D.J. Morrissey, R. Pfaff, B.M. Sherrill and M. Steiner

In the past few years projectile fragmentation at high (E > 200 MeV/nucleon) and intermediate (between 20 and 200 MeV/nucleon) energies has been proven to be an effective method to produce a broad range of exotic nuclei. Whereas the production mechanism leading to exotic nuclei seems to be well understood at high energies, little is known about the reaction mechanisms at intermediate energies. In the later energy domain it is believed that a gradual transition occurs between transfer-, and fusion-evaporation reactions, that dominate the low energy regime (E < 20 MeV/nucleon), and the pure fragmentation reactions dominating at high energies. In order to obtain further insight into the competing reaction mechanisms at intermediate energies we performed a short measurement with an exotic beam, in which our goal was not to search for new isotopes, but to measure the production cross sections of various neutron rich fragments and compare the results to experimental data taken at higher bombarding energies [1], to the predictions of an intranuclear cascade model (INC) [2] and to a semi-empirical parameterization [3].

A 100 MeV/nucleon ^{48}Ca beam from the K1200 cyclotron irradiated a 284 mg/cm^2 ^{9}Be target located at the medium acceptance target position of the A1200 fragment separator [4]. The A1200 was operated in the maximum momentum acceptance mode of $\Delta p/p = \pm 1.5\%$. The experimental setup and analysis procedures used for this experiment were similar to those described in Ref. [5] and therefore should not be described here.

We measured the production cross sections for 36 neutron-rich isotopes ranging from Z=19 (potassium) to Z=9 (fluorine). The data was obtained by integrating a gaussian fit to the parallel momentum distributions, and correcting these results for the acceptance of the A1200 fragment separator using the code INTENSITY [6].

A comparison of the production cross sections obtained in this experiment (solid circles) to those from an experiment performed at roughly twice the beam energy [1] (open squares) is shown in Fig.1. The overall agreement between both experiments is excellent. As for beam energies above 200 MeV/nucleon pure fragmentation is assumed to be the only production mechanism for projectile like residues, the very good agreement between the two experiments seems to indicate that pure fragmentation is still the dominant reaction mechanism at 100 MeV/nucleon. However, due to the lack of experimental data taken at 213 MeV/nucleon for residues very close to the projectile one cannot rule out the existence of other reaction mechanisms completely. Especially as the residues close to the projectile are the most sensitive ones to different types of reaction mechanisms. If transfer reactions play an important role for nucleus-nucleus collisions at 100 MeV/nucleon, one expects to find a larger yield for fragments very close to the projectile in the present data compared to the experiment performed at 213 MeV/nucleon.

We can also compare the production cross sections obtained in this experiment to the predictions of the microscopic model ISApace [2] and to the semi-empirical parameterization EPAX [3]. ISApace combines the intranuclear cascade code ISABEL [7] with the evaporation code PACE [8]. ISApace has been successfully used to reproduce high energy fragmentation data and is believed to give a rather accurate description of the reaction mechanism (pure fragmentation) involved in peripheral nucleus-nucleus collisions at relativistic energies. However, due to its Monte Carlo basis, ISApace is not well suited to the low cross section of isotopes far away from the valley of stability. EPAX on the other hand is a semi-empirical, analytical parameterization obtained by Sümmerer, et al. [3] from a compilation of

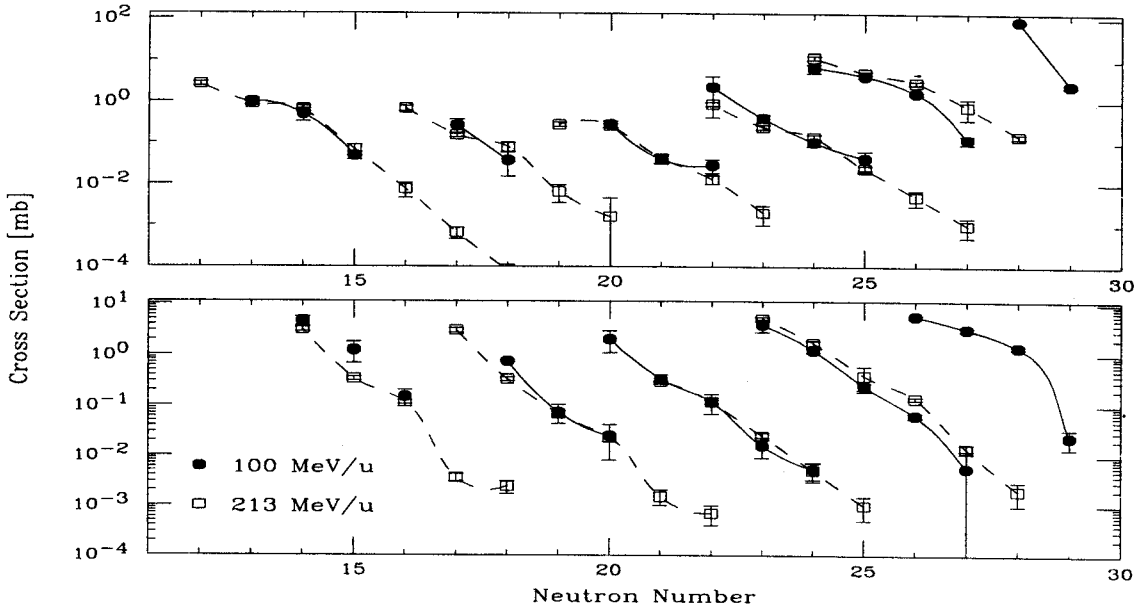

Figure 1: Comparison of the production cross sections of different neutron-rich isotopes.For clarity we display the elements with odd element number (Z=9 to Z=19) in the upper panel and those with even element number (Z=10 to Z=18) in the lower panel. The solid points indicate the cross sections from this experiment, the open squares represent production cross sections taken at roughly twice the incident energy [1].The lines are drawn to guide the eye.

high energy target and projectile fragmentation data, that is able to predict the production cross sections of all residues.

The overall agreement of the experimental data with both ISApace and EPAX is very good, as can be seen in Fig. 2. We note that there is a deviation between the theoretical predictions and the measured cross sections for the isotopes very close to the projectile. The experimental cross sections are clearly higher than those predicted by both theoretical models. This seems to be an indication that transfer reactions play a role for nucleus-nucleus collisions at 100 MeV/nucleon. However, due to the lack of experimental data taken at higher incident energies, we can only see this as an indication, but not as a proof, of the presence of other reaction mechanism than pure fragmentation.

The comparison of the production cross sections of neutron rich fragments taken at 100 MeV/nucleon to data taken at 213 MeV/nucleon, and to two models known to be valid for high energy fragmentation reactions show very good agreement. This indicates that pure fragmentation is still the dominant reaction mechanism for the production of projectile like residues at 100 MeV/nucleon. The underestimation of the cross sections of residues close to the projectile by both theoretical models seems to indicate that other reaction mechanism might still be effective. However, the lack of any reaction products heavier than the projectile clearly shows that these processes just play a minor role. For further studies a comparison to data taken at lower energies is of great interest. Some experiments (see e.g. [9,10]) have already been performed at about 50 MeV/nucleon. However these experiments were solely

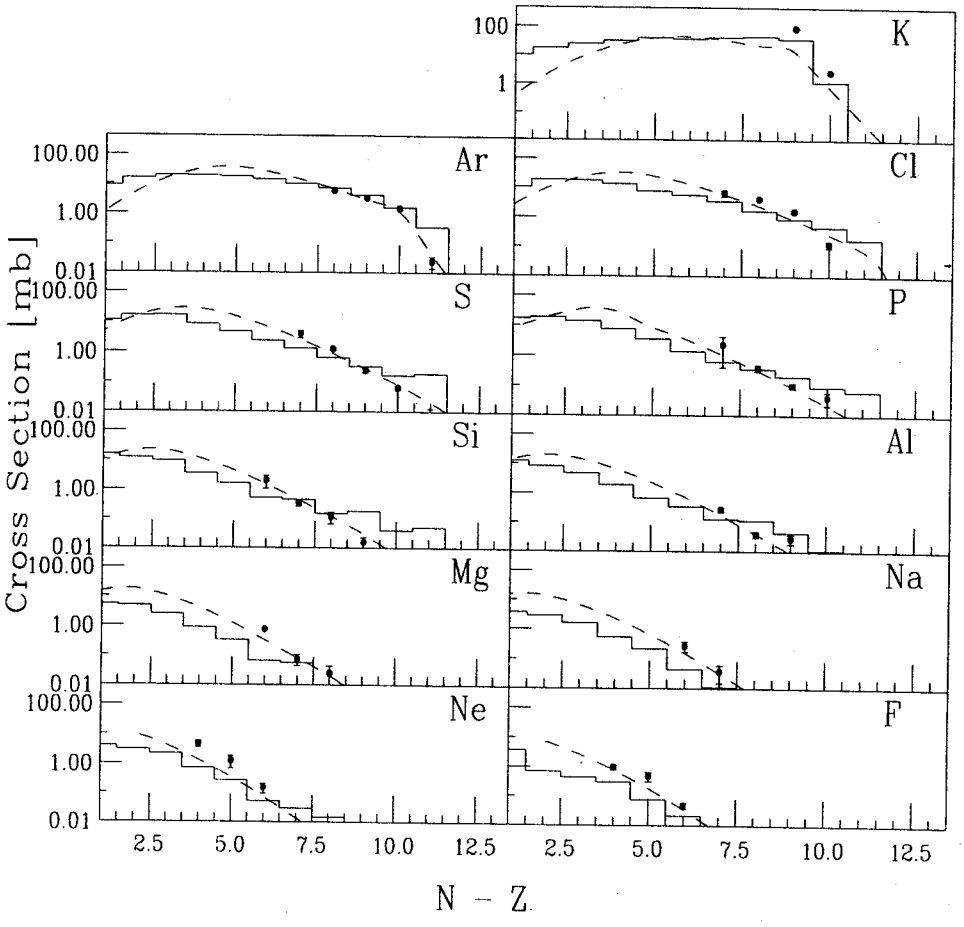

Figure 2: Isotopic distributions for the elements between potassium (Z=19) and fluorine (Z=9). The solid points represent the experimental data of this work. The histogram is the result of a corresponding ISApace [2] calculation, whereas the dotted line represents the semi-empirical formula EPAX [3].

aimed to search for new isotopes and did not map out the (parallel) momentum distributions and thus cannot report any production cross sections of fragments.

We hope to continue our studies in the future and to extend the production yield measurements to lower energies and thus to map out the importance of different reaction mechanisms at intermediate energies. This. knowledge is very important for the planning of future experiments with radioactive beams and should lead to a parameterization similar to that of Sümmerer et al., valid for the intermediate energy regime

References

1. G.D. Westfall, et al., Phys. Rev. Letters **43** (1979) 1859.
2. M. Fauerbach, Diploma Thesis, TH Darmstadt (1992).
3. K. Sümmerer, et al., Phys. Rev. **C42** (1990) 2546.
4. B.M. Sherrill et al. Nucl. Instr. Methods **B56** (1991) 1106.
5. R. Pfaff et al., Phys. Rev. **C51** (1995) 1348.
6. J.A. Winger, B.M. Sherrill and D.J. Morrissey, Nucl. Instr.. **B70** (1992) 380.
7. Y. Yariv and Z. Fraenkel, Phys. Rev. **C20** (1979) 2227.
8. A. Gavron, Phys. Rev. **C21** (1980) 230.
9. D. Guillemaud-Mueller et al., Zeit. fuer Phys. **A322** (1989) 189.
10. M. Lewitowicz et al., Zeit. fuer Phys. **A335** (1990) 117.

SEARCH FOR THE GROUND STATE OF ^{11}N

A. Azhari, T. Baumann, J.A. Brown, M. Hellström, J.H. Kelley, R.A. Kryger, E. Ramakrishnan, M. Thoennessen, T. Suomijarvi, S. Yokoyama, H. Madani[a], D. Russ[a]

The study of nuclei beyond the drip lines is of high current interest. Careful studies of these nuclei can provide us with a better understanding of nuclear structure in general. With the availability of radioactive nuclear beams, the task of studying these exotic nuclei has become more feasible. These particle unbound nuclei can be produced via transfer reactions with radioactive beams. These nuclei then rapidly decay by emitting a proton or a neutron. By observing the decay particle and the daughter nucleus in coincidence, the states of these unbound nuclei can be reconstructed.

In a recent experiment we studied the decay characteristics of ^{12}O[1]. This nucleus was predicted to be a diproton emitter, decaying by emitting a ^{2}He. Analysis of the data, however, determined an upper limit of only 7% for the ^{2}He decay branch. Therefore, another possible decay branch, sequential one proton decay, was considered. This would require that the ^{12}O decays to ^{10}C via an intermediate state in ^{11}N. A state in ^{11}N has been observed at a decay energy of 2.24 MeV and G = 740 keV[2]. However this state was interpreted to be the isobaric analogue of the 1/2$^-$ first excited state in ^{11}Be. Isobaric Mass Multiplet Equation (IMME) calculations have predicted the analogue of the 1/2$^+$ ground state of ^{11}Be in ^{11}N to be 300 keV lower, at a decay energy of 1.9 MeV. This would be an s-wave state, therefore, it is also predicted to be much more wider than the 740 keV width of the p-wave excited state.

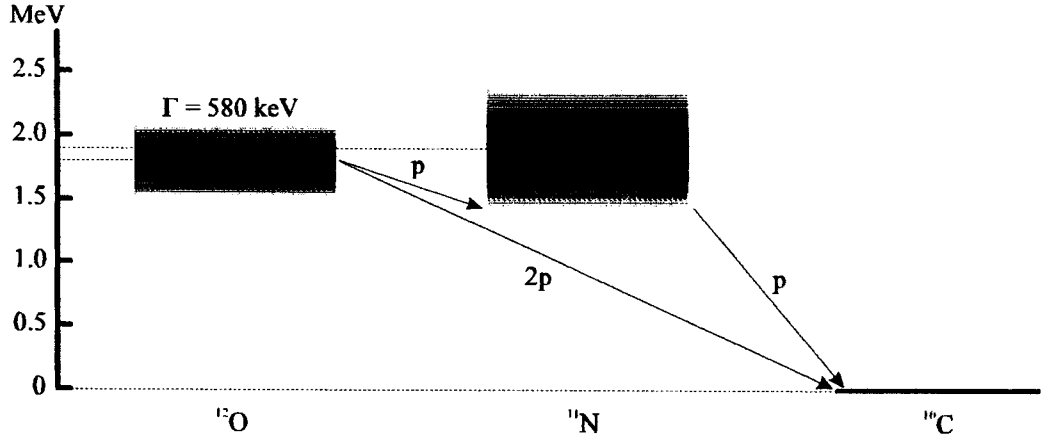

Fig. 1: ^{12}O can decay by emitting a ^{2}He directly to the ground state of ^{10}C. A possible alternative would be the sequential one proton decay through the tail of the predicted 1.9 MeV ground state of ^{11}N.

Figure 1 shows the two decay schemes mentioned above. Although the data pointed strongly towards the sequential one proton decay mode, this decay branch would be suppressed if the ground state of ^{11}N is at 1.9 MeV. Penetrability calculations for this scenario show that the decay would proceed predominantly through the lower tail of this ground state at a point where the energy of the two protons emitted would almost be equal. This would suppress the decay and result in a small width for the ground state of ^{12}O, inconsistent with the measured width of 580 keV. The possibility of the existence of a state in ^{11}N lower than the 1.9 MeV was considered and the data was consistent with a state near 900 keV. This is much lower than anticipated, therefore, better measurements of the ^{11}N system were required to shed more light on this inconsistency.

We performed an experiment at the NSCL to study ^{11}N. A primary beam of 80 MeV/A ^{16}O from the K1200 was used in a fragmentation reaction on a thick (1000 mg/cm^2) ^{9}Be target to produce the

radioactive beam of ^{12}N. The A1200 mass separator followed by a velocity filter (RPMS) resulted in a ^{12}N beam of better than 95% purity on the secondary target. A primary beam intensity of ~200 pnA yielded ~15000 cps of 40 MeV/A ^{12}N on target at the tail of the RPMS. Two Parallel Plate Avalanche Counters (PPACs) were placed before the secondary 36 mg/cm^2 ^9Be target in order to provide beam trajectory information. The ^{11}N was produced via single neutron stripping/transfer reaction $^9Be(^{12}N, ^{11}N)$ decaying almost immediately to ^{10}C by emitting a proton.

The protons were detected in the Maryland Forward Array which was placed about 20 cm behind the target. This array consisted of a 300 mm annular silicon detector with 16 segments on the back and 16 radial strips in quadrants on the front which was then backed by a ring of 16 plastic phoswich detectors. The annular silicon detector provided us with position resolution and DE measurements, while the plastic phoswich detectors were used for particle identification via fast vs. slow pulse discrimination, and also measured the energy.

The ^{10}C fragments from the decay of ^{11}N, were more forward focused, which allowed them to pass through the central hole in the proton detectors. These particles were detected in a PPAC-DE-E telescope placed 62 cm downstream of the target, directly at 0°. This telescope consisted of a 5 cm x 5 cm PPAC backed by a 5 cm x 5 cm 500 mm thick quadrant silicon detector followed by a 6.5 cm diameter 3 mm thick Si(Li) detector with four pie-shaped segments. This arrangement provided us with the position, DE, and E information.

To calibrate the proton detectors, molecular beams at two different energies were tuned and passed through a stripper foil to produce protons at energies of 75 MeV and 30 MeV. These protons were then transmitted to the tail of the RPMS where an arrangement of degraders allowed us to degrade these protons to several desired energies ranging from 10 to 75 MeV. A thin gold foil was then used to elastically scatter the protons into all the proton detectors. For these measurements, a thick block of copper was used to shield the fragment telescope from the protons to avoid any damage to the silicon detectors.

The fragment telescope was calibrated by tuning ^{10}C and ^{11}C fragments produced at the primary target, at the beginning of the A1200, to the tail of the RPMS. A different set of degraders was then used to degrade these beams, thus obtaining an adequate number of calibration points for carbon isotopes of interest.

The measured energies for the protons and the ^{10}C fragments seen in coincidence, and the lab frame opening angle between them allow us to reconstruct the decay energy of the ^{11}N states which were populated. Figure 2 shows the result of this reconstruction for ^{11}N.

In order to interpret the data, Monte Carlo simulations of the experiment were performed. These simulations incorporated experimental conditions such as the beam characteristics, target thickness, and decay parameters for ^{11}N. Also included in these calculations were geometric efficiencies and resolutions of the detectors. Included in Figure 2, the dashed peak at about 2 MeV, is a simulation of the known 2.2 MeV, G = 740 keV excited state of ^{11}N. The smaller dashed peak at about 4 MeV is a simulation of the higher excited states of ^{11}N where a 1.0 MeV wide state was considered at 4.0 MeV decay energy in order to simulate their effects in the lower decay energy regions. Since the geometric efficiency in this region is low, individual states can not be separated. The effect of these higher excited states in the region of interest, at or below 2.5 MeV, is minimal. It is clear that the 2.2 MeV and the 4.0 MeV states can not reproduce the shoulder on the low energy side of the data. Therefore there must be at least one other state present in this region. A simulation for a 1.2 MeV, G = 1.0 MeV state resulted in the dotted peak. In order to determine the relative contribution from each of these states, normalization factors were derived which gave the best fit not only to the decay energy spectrum, but other experimental observables such as proton energy, fragment energy, and opening angle between the protons and the ^{10}C fragments. Once these normalization factors were determined, the three simulated

spectra were summed to produce the solid line. The sum of these spectra reproduces the data very well.

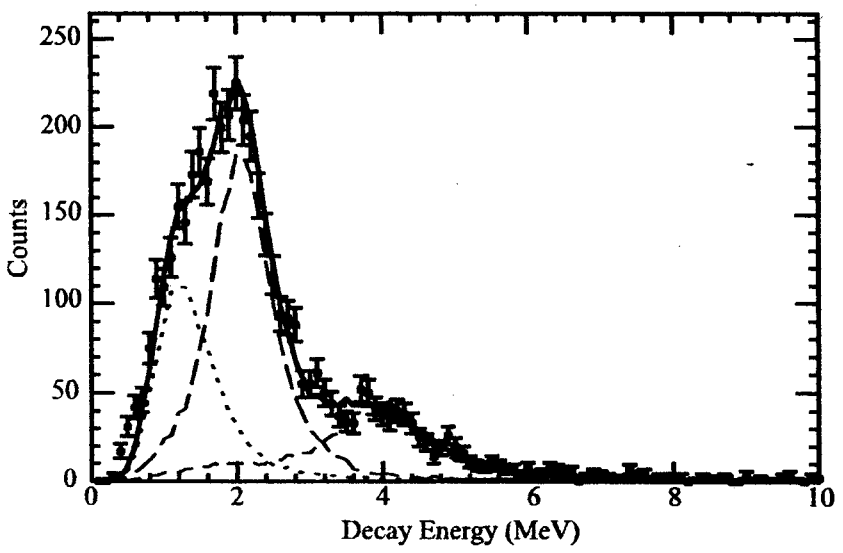

Fig. 2: Decay energy spectrum for ^{11}N. The points with error bars represent the data. The dotted line is a simulation of a 1.2 MeV state with G = 1.0 MeV, the dashed line is a simulation of the known 2.2 MeV state G = 740 keV. Also included is a simulation of a state at 4.0 MeV with G = 1.0 MeV (the smaller dashes). The solid line is a sum of all three components.

In conclusion, we have observed protons in coincidence with ^{10}C nuclei from the decay of ^{11}N and have located the known 2.2 MeV excited state of ^{11}N. We have also observed evidence for a state in ^{11}N which lies lower than the known 2.2 MeV excited state, but, this state is considerably lower than the previously predicted ground state value of 1.9 MeV. Further analysis is under way.

a. Department of Chemistry, University of Maryland.

References

1. R.A. Kryger et. al., Phys. Rev. Let. **74**, 860 (1995)
2. W. Benenson et. al., Phys. Rev. C **9**, 2130 (1974)

PRODUCTION OF ^{6,7}Li AND ^{7}Be IN $\alpha + \alpha$ REACTIONS ABOVE 40 MeV/NUCLEON

D. J. Mercer[a], Sam M. Austin, J. A. Brown, S. A. Danczyk, S. E. Hirzebruch, J. H. Kelley, D. A. Roberts[b], and T. Suomijärvi

We seek to measure the cross sections for production of ^{6}Li, ^{7}Li and ^{7}Be when a target of ^{4}He is bombarded with α particles at energies of 40, 70, or 155 MeV/nucleon.

The cross sections are needed to calculate limits of galactic cosmic ray (GCR) production of $A = 6, 7$ isotopes. The isotope ^{6}Li is of particular interest to cosmology because it is not made in appreciable quantities in the standard Big Bang model or in stellar processes [1], yet has been recently observed in ancient Population II stars in our galaxy [2]. Cosmic ray α particles fusing with primordial helium give one plausible mechanism for ^{6}Li production. The $A = 7$ isotopes are also of interest because the Big Bang model is constrained to produce any quantities that are not accounted for by other means, which includes GCR nucleosynthesis.

Calculations for GCR $A = 6, 7$ production use the available measurements for the $\alpha + \alpha$ cross sections, which are shown in Figure 1. No published measurements exist above 50 MeV/nucleon, although unpublished limits for $A = 7$ are available. It is not known whether the cross section for ^{6}Li continues to fall (as for $A = 7$) or remains near its value at 50 MeV/nucleon, resulting in a factor 3 uncertainty in total GCR production rates. During NSCL experiment 93024 we have collected data at 40, 70, and 155 MeV/nucleon. When analysis is complete, we expect these data will resolve the factor 3 uncertainty.

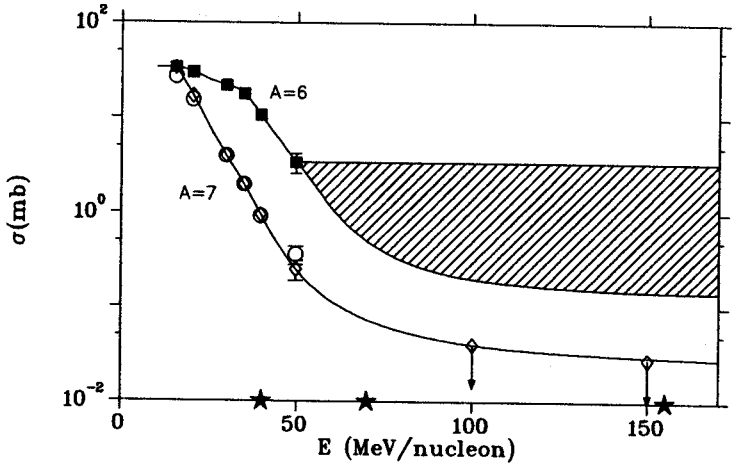

Figure 1: Cross section measurements from Refs. [3-6] for $A = 6, 7$ production in the $\alpha + \alpha$ reaction. Stars indicate beam energies for which we have collected new data, and the shaded region shows the uncertainty we hope to resolve. Normally the curve parallel to the A=7 curve is used in calculations.

A novel experimental technique is used which eliminates the traditional helium gas cell target, thereby reducing background scattering from target windows. The 13 m^3 volume of the NSCL 92-inch scattering chamber is filled with helium gas at 400 torr, and detector telescopes are placed inside the gas volume. Two telescopes are used, each a sandwich of two position-sensitive silicon strip detectors approximately 1 × 9 cm^2 (Micron Design TT or Orsay models) and a CsI(Tl) scintillator. These telescopes

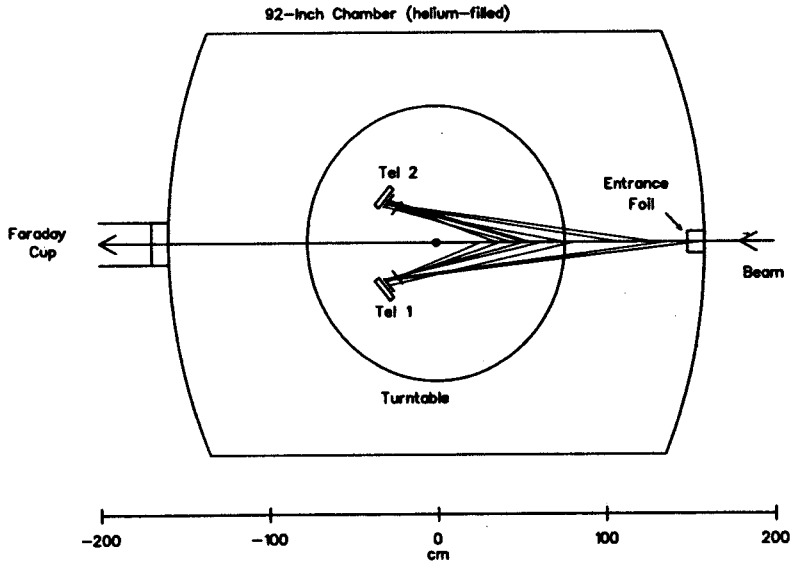

Figure 2: The experimental setup, showing the two angle-sensitive telescopes and several reconstructed ^{6}Li tracks from the 40 MeV/nucleon $\alpha + \alpha$ reaction.

provide identification of ^{6,7}Li and ^{7}Be as well as sensitivity to the scattering angle θ_{lab} of the particle. The telescopes each cover more than 25° of angular range, and are mounted on a turntable to further expand the range and serve as a cross-check of acceptance. A schematic of the setup appears in Figure 2, along with some typical reconstructed ^{6}Li tracks.

Data were collected for θ_{lab} as small as 5°, which due to the "folded" kinematics of the fusion reaction determines both the maximum and minimum center-of-momentum angle. A typical θ_{cm} range for data collected is 15-140°. The measured angle resolution for each telescope is 1.6° FWHM in θ_{lab}. Data will be binned by angle and integrated over the entire θ_{cm} range to provide total cross sections, with necessary extrapolations for large and small angles causing an uncertainty of about 20%. Approximately 40,000 counts of ^{6}Li were collected at 40 MeV/nucleon, of which approximately 0.6% are background events from the entrance foil of the 92-inch chamber. Approximately 18,000 counts of ^{6}Li were collected at 70 MeV/nucleon, and 2,500 counts at 155 MeV/nucleon, for which background events are a larger and as yet undetermined fraction. Analysis is continuing at the University of Colorado.

a. Department of Physics, University of Colorado, Boulder, CO 80309-0446
b. Department of Physics, University of Michigan, Ann Arbor, MI 48109-1120

References

1. G. Steigman and T.P. Walker, Astrophys. J. 382, L13 (1992).
2. V.V. Smith, D.L. Lambert, and P.E. Nissen, Astrophys. J. 408, 626 (1993).
3. B.G. Glagola, V.E. Viola, Jr., H. Breuer, N.S. Chant, A. Nadasen, P.G. Roos, S.M. Austin, and G.J. Mathews, Phys. Rev. C 25, 34 (1982).
4. L.W. Woo, K. Kwiatkowski, S.H. Zhou, and V.E. Viola, Jr., Phys. Rev. C 32, 706 (1985).
5. L.W. Woo, K. Kwiatkowski, T.E. Ward, and V.E. Viola, Jr., Indiana Nuclear Chemistry Report INC-40007-14 (1982).
6. F. Yiou and G.M. Raisbeck, in *Proceedings of the 15th International Cosmic Ray Conference,* (Plovdiv, Bulgaria, 1977) O.G. 133.

MEASUREMENT OF (p,n) REACTIONS IN INVERSE KINEMATICS

J. A. Brown, D. Bazin, W. Benenson, J. Caggiano, M. Fauerbach, M. Hellström[a], J. H. Kelley, R. A. Kryger[b], B. M. Sherrill, M. Steiner, D. J. Morrissey, R. Pfaff, and C. F. Powell.

The recent development of high intensity secondary beams has allowed new studies of the structure of many unstable nuclei. While particular effort has been focused on measuring breakup cross sections and momentum distributions of halo nuclei, there is growing interest in investigating the detailed structure of these and other unstable nuclei using well understood tools developed to study stable nuclei. Direct nuclear reactions, (p,n), (p,p'), and transfer reactions have traditionally been used to measure important quantities in nuclear structure physics, such as weak-interaction transition strengths, energy levels and nuclear matter density distributions. These types of measurements have up to now been very difficult to perform with unstable nuclei, due to the impossibility of constructing a radioactive target from any short-lived isotopes. The use of inverse kinematics with secondary radioactive beams of very short lived nuclei is a general tool for studying these types of reactions. We have developed a new method to study the (p,n) reaction in inverse kinematics at the NSCL.

Proton induced (p,n) reactions have been used extensively to probe weak-interaction strengths. At 0°, the (p,n) cross-section is proportional to the weak-interaction transition strength between the ground state of e nucleus $^{A}(Z)$ and states in the nucleus $^{A}(Z+1)$, denoted B(GT) and B(F) for Gamow-Teller and Fermi transitions respectively [1]. The (p,n) reaction is an effective probe of the difference in neutron and proton density distribution [2]. This should be particularly useful in neutron halo nuclei where the neutron density distribution decreases much more slowly at large radii than does the proton distribution[3]. Proton induced (p,n) reactions have been studied on a great many stable targets [4]. From these experiments, extensive systematics have been developed [1,4]. The limitation of stable targets has constrained (p,n) work to the valley of β-stability. We have used the A1200 fragment separator to develop secondary β-unstable nuclear beams and study the (p,n) reaction with these nuclei. Using the A1200 as a dispersion-matched energy loss spectrometer to detect the heavy ion constrains this type of experiment in other and equally profound ways. Only particle stable states of the ejectile nucleus can be observed, and the energy resolution of the experiment worsens linearly with the projectile mass. The ultimate resolution of these experiments will be limited by three major contributions: the ion optical resolution of the A1200, the ability to reconstruct scattering angles to correct for the kinematic shift, and the target thickness needed to get an acceptable counting rate.

Used as a dispersion-matched energy loss spectrometer, the A1200 has a theoretical momentum resolution of 2000 with a 1 mm beam spot on the production target [5,6]. However, in normal operation the resolution is often closer to 1600. Figure 1 shows how this finite momentum resolution affects the experimental resolution for beam energies of E/A = 80, 100, and 120 MeV. This limits the useful mass range for (p,n) reactions in inverse kinematics to masses less than about sixty in order to keep the resolution to below 4 MeV. The absolute resolution worsens simply due to the increase in total beam energy with projectile mass.

An additional limit on the resolution is the strong kinematic shift of the heavy ion with laboratory scattering angle, as shown in figure 2. The initial angular acceptance of the A1200 can be limited, and the angular resolution achievable at the focal plane is near 1.5 mr. After adjusting for the angular magnification of the A1200, the initial beam divergence is still the limiting factor in the reconstruction of scattering angles at the focal plane. Thus, the recoil energy can only be reconstructed to a resolution:

$$\Delta E = \left.\frac{\partial E}{\partial \theta_{c.m.}}\right|_{\theta_{c.m}} \Delta\theta.$$

The use of a CH_2 target also will usually require background subtraction for an equivalent thickness and time using a natural carbon target. For lighter ions, this a less of a problem, as the resolution is still much better than the difference of the Q-values between a (p,n) reaction and carbon induced charge exchange reactions is nearly 10 MeV.

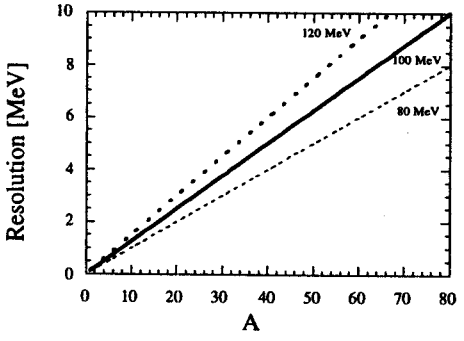

Figure 1: Ion optical resolution of the A1200 as a function of projectile mass. Assuming a 1mm beam spot, at E/A of 80, 100 and 120 MeV

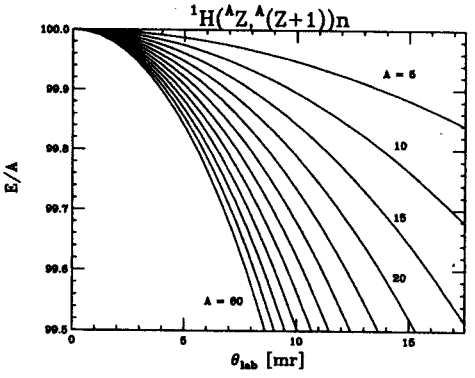

Figure 2: Kinematic shift of the heavy ion at E/A 100 MeV, for a p(^{A}(Z),^{A}(Z+1)) reaction with Q=0 .

The reaction ^{1}H(^{6}He,^{6}Li)n is particularly useful for testing this technique. There are two particle stable states in the nucleus ^{6}Li which are likely to be populated. The limit on the resolution due to the uncertainty in the scattering angle combined with the kinematic shift of the heavy ion is still not too strong, ~150 keV. The nucleus ^{6}He is a known two neutron halo nucleus, and further detailed analysis should allow the differential cross sections for (p,n) to be compared to the (p,p') angular distribution to deduce the difference between the proton and neutron density distributions. For this reaction, the kinematics were fairly simple to correct for, as shown in figure 3. There are three particle stable states in the nucleus ^{6}Li: the 1^+ ground state, the 3^+ first excited state at 2.186 MeV and the 0^+ second excited state at 3.563 MeV. The 0^+ state is the isobaric analog of the ground state of the ^{6}He nucleus. Only the ground state and the isobaric analog should be strongly populated by a (p,n) reaction near 0°, as here (p,n) is (ΔT=1, and ΔS=0,1). The ground state will be populated through a Gamow-Teller transition and the 2nd excited state by a Fermi transition.

Using a primary beam of ^{7}Li at E/A=90 MeV incident on a 470 mg/cm^2 Be target at the low acceptance position of the A1200, a secondary beam of ^{6}He at E/A=93 MeV was produced. This beam was directed onto a n 18 mg/cm^2 CH_2 target at the second dispersive image, while the third segment of the A1200 was set to collect the ^{6}Li ions from the ^{1}H(^{6}He,^{6}Li) reaction. In this optical mode, the A1200 focus from the second dispersive image is point-to-point in the horizontal direction and point-to-parallel in the vertical direction. By using two cathode readout drift chambers, a position sensitive silicon detector and a fast plastic scintitilator, the position, angle, energy, and particle type could be determined at the focal plane. The vertical position is proportional to vertical scattering angle, and the horizontal scattering is reconstructed using the three horizontal position measurements. The reconstructed energy spectrum is shown in figure 4.

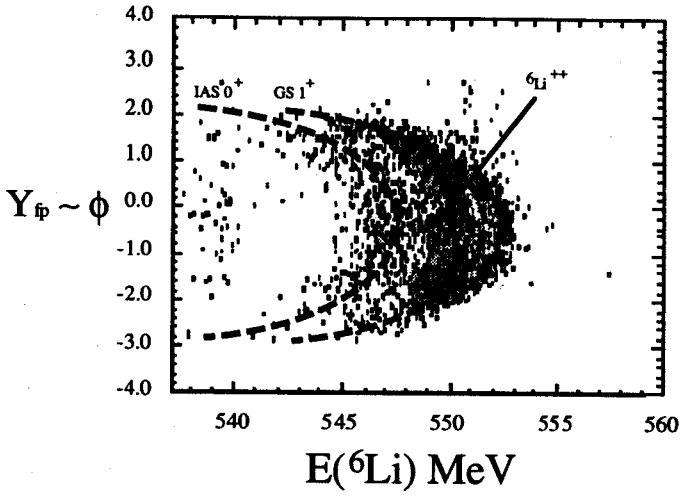

Figure 3: The kinematic shift of the $^{1}H(^{6}He,^{6}Li)n$ reaction observed at the A1200 focal plane. The ground state and the second excited state are clearly visible as parabolas due to the kinematic shift with scattering angle. Here ϕ is the vertical scattering angle.

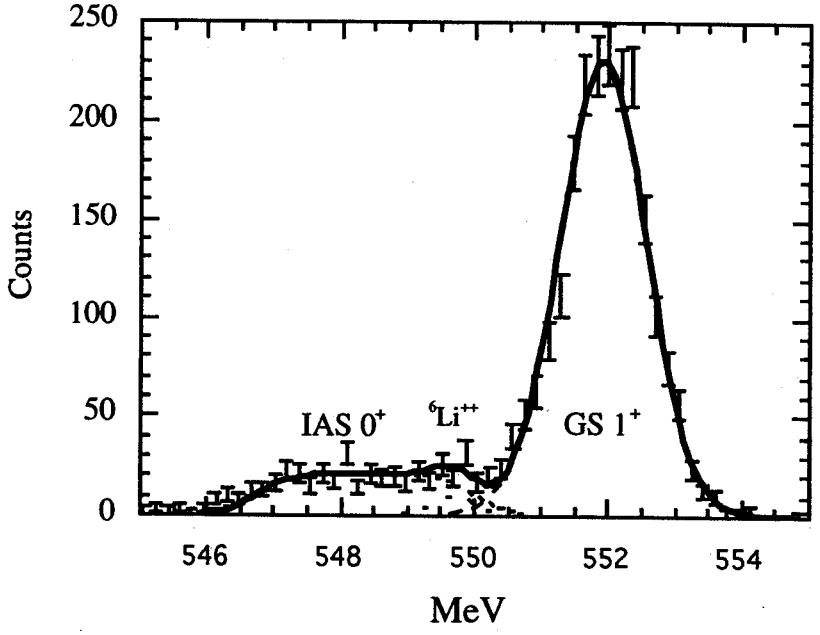

Figure 4: After correcting for the kinematic shift, a resolution of 900 keV is achieved, $P/\Delta P = 1200$. The IAS is broadened by 1.53 MeV due to γ-ray emission. The solid curve shows the total fit and the dashed curves show the contributions of individual components.

B(GT) values can be extracted from the differential cross section at 0° a for Gamow-Teller transition by using a nearby Fermi transition. In this case, we chose to use the Fermi transition from the ground state of ^{6}He to the second excited of ^{6}Li: (0^{+}, 3.563 MeV). The B(GT) value can be found from systematics, as

$$R^2 = \frac{\sigma_{GT}(0°)}{\sigma_F(0°)} \frac{N-Z}{B(GT)} \frac{K\left(Q-E_F\right)}{K\left(Q-E_{GT}\right)}$$

where $K(Q\text{-}E)$ is a kinematic factor. This factor arises from the different momentum transfer for the two states at 0°, due to the difference in excitation energy. From systematics, R can be parameterized as

$$R(E_p) = \frac{E_p}{E_0}$$

with E_0=55.0±0.4 MeV [1].

Limiting Θ_{cm}<~12° and interpolating the relative strengths to 0°, R_{exp}=1.521±0.045 is found by using the known B(GT) value from β-decay and (n,p), which compares to a systematic value R_{sys}=1.689±.018. Thus, this experiment is able to reproduce (81±14)% of the known Gamow-Teller strength for the transition from ^{6}He to the ground state of ^{6}Li.

The results of this experiment are quite encouraging, and have clearly demonstrated the viability of the inverse kinematic technique for (p,n) reactions with light nuclei. A great deal of interesting physics is now explorable by complementary techniques. The neutron halo can be probed not only by measuring momentum distributions and removal cross sections, it can also be examined by charge exchange. However, there are still difficult problems to overcome in extending this method to heavier nuclei. In the future, many of the constraints on this technique will be much less severe when the S-800 spectrometer can be used. With the improved momentum resolution (20,000) [7] of the S-800, this technique should be extended into the much more interesting A~60 region. In that mass region, the strength of weak interaction transitions determines some of the important parameters in supernovae precursors: the electron fraction, and the rate of core cooling due to neutrino loss.

a. Present address: Gesellschaft für Schwerionenforschung, D-64220 Darmstadt, Germany
b. Present address: Florida Flavors Inc., 4330 Drain Field Road Lakeland, FL 33811

References

1. T. N. Taddeucci, et al., Nuclear Physics A469, (1987) 125-172
2. R. Satchler and W. G. Love, Physics Reports 55, (1979) 183
3. I.Tanihata, et al., Physical Review Letters 55, (1985) 2676
4. C. D. Goodman, et al., Physical Review Letters 44, (1980) 1755-9
5. B. M. Sherill et al., Nuclear Instruments and Methods B 56&57, (1991) 1106
6. B.L. Cohen, Review of Scientific Instruments 30, (1959) 415
7. B. M. Sherrill, et al., S-800 Proposal, MSUCL-694

GIANT DIPOLE RESONANCE IN HIGHLY EXCITED ^{120}Sn AND ^{208}Pb NUCLEI POPULATED BY INELASTIC ALPHA SCATTERING

E. Ramakrishnan, T. Baumann, A. Azhari, R. A. Kryger, R. Pfaff, M. Thoennessen, S. Yokoyama, J.R. Beene[a], F.E. Bertrand[a], M.L. Halbert[a], P.E. Mueller[a], D.W. Stracener[a], R.L. Varner[a], G. Van Buren[b], R.J. Charity[b], J.F. Dempsey[b], P-F. Hua[b], D.G. Sarantites[b] and L.G. Sobotka[b].

The study of giant dipole resonance (GDR) built on excited states of the nucleus can convey information on nuclear properties at high temperatures. The GDR couples strongly to the shape degrees of freedom of the nucleus. The resonance is thus sensitive to changes in the nuclear potential surface that arise from temperature and spin. The evolution of the GDR in hot nuclei has been studied primarily by means of fusion-evaporation reactions [1]. Fusion measurements in highly excited *Sn* isotopes have observed a systematic increase in the width of the resonance with excitation energy [2,3]. However, the increase in excitation energy is associated with an increase in the angular momentum transferred to the compound nucleus [4]. It is not easy to decouple the effects of temperature and spin in fusion measurements in the study of resonance properties at high excitation energies.

An alternative to fusion reactions is to excite the nucleus of interest by light ion inelastic scattering. Low angular momentum states are populated in the inelastic scattering process and the resonance properties can be studied as a function of excitation energy with very little influence from angular momentum.

We studied the GDR built on highly excited states of ^{120}Sn and ^{208}Pb nuclei. Inelastic α scattering at 40 and 50 MeV/nucleon was used to excite the target nuclei and the GDR was studied by measuring the high energy γ-rays from the decay of the resonance in coincidence with the outgoing projectile nuclei. The γ rays were measured in 95 BaF_2 detectors arranged in 5 close-packed arrays of 19 detectors each, at laboratory angles of $\sim 60°$ and $\sim 115°$. The inelastically scattered projectile nuclei and other light charged reaction products were measured in the *DWARF Ball/Wall* 4π CsI array which consisted of 99 detectors covering laboratory angles of $\sim 10°$ to $\sim 155°$ [5]. Target excitation energies of up to 110 MeV in ^{208}Pb and up to 130 MeV in ^{120}Sn were selected by gating on the energy loss of the projectile nuclei.

Contributions to the inelastic continuum from background processes like nucleon knockout, nucleon pickup and sequential decay were estimated to be of the order of 20%. Such processes contribute to the measured singles cross section, but do not contribute to the coincidence γ-ray spectra since the target nucleus is not excited.

The inelastic α spectra in coincidence with γ-rays of energy greater than $\sim$4 MeV exhibited structures that corresponded to individual neutron evaporation channels in the decay of the excited nucleus. This was evidence for equilibrated emission from a highly excited target nucleus.

The γ-ray spectra in coincidence with the inelastically scattered projectile nuclei were extracted for various '10 MeV wide' target excitation energy ranges. The spectra were analysed within the standard statistical model. Calculations were performed with a modified version of the statistical evaporation code CASCADE. An energy dependent level density parametrization was applied to both systems. The input population for the statistical model calculations was derived from the particle singles spectrum.

Figure 1 displays the γ-ray spectra from the two targets for a typical excitation energy of 60-69 MeV. The top panels display the data along with the statistical model calculations. The bottom panel displays the same data and calculation on a linear scale. This was achieved by dividing the data and the

calculation by a second statistical calculation that employed an energy independent E1 strength function.

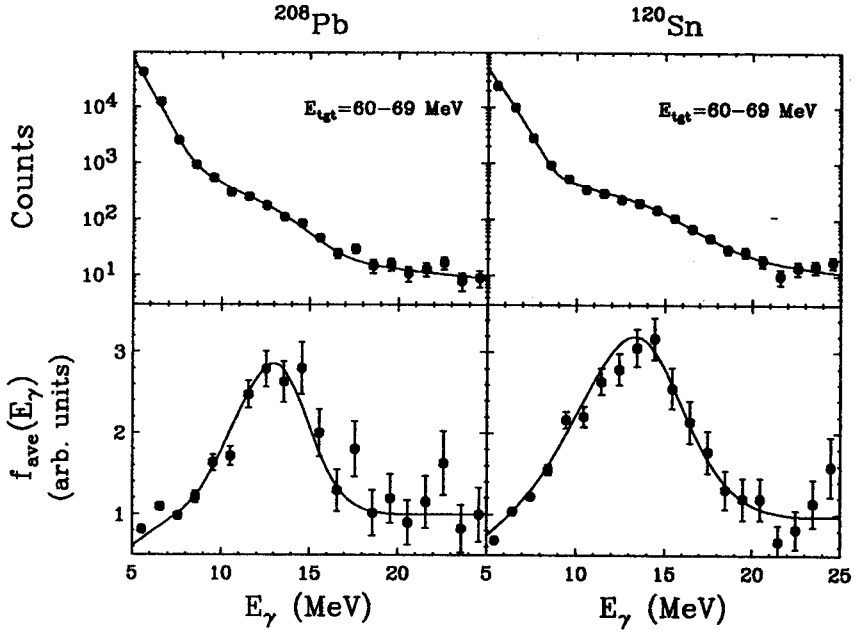

Figure 1: Coincidence γ-ray spectra (filled circles) and statistical model calculations (solid line) for ^{208}Pb and ^{120}Sn at excitation energies of 60–69 MeV. The top panels display the measured spectra and calculations. The bottom panel display the data and the calculations on a linear scale, obtained as explained in text.

The resonance parameters were extracted as a function of target excitation energy from fits to the data performed with the statistical model calculations. A resonance energy value of 15.0 MeV was extracted for ^{208}Pb. This value is ~1.5 MeV above the ground state resonance energy [6]. No systematic dependence was observed as a function of target excitation energy. In ^{120}Sn, the extracted resonance energy varied from ~16 MeV to ~14 MeV with increasing excitation energy, the ground state value being 15.4 MeV [6].

The sum rule strength extracted from fits to the ^{208}Pb data was observed to decrease from ~ 100% to ~ 50% with increasing excitation energy. This could be due to processes in the inelastic scattering that did not excite the collective dipole resonance but resulted in the emission of γ rays below ~8 MeV. In ^{120}Sn, a sum rule strength close to 100% was extracted.

The width of the GDR was observed to increase systematically with increasing excitation energy in both systems. The width increased from the ground state value to ~ 8MeV in ^{208}Pb and to ~ 12 MeV in ^{120}Sn at the highest measured excitation energy.

The giant dipole resonance width in nuclei consists of two components, the escape width ($\Gamma^{\uparrow}$) and the spreading width ($\Gamma^{\downarrow}$). The escape width arises from the coupling of the resonance to particle decay channels and is of the order of a few hundred keV. Thus the main contribution to the resonance width is from the spreading width, which is due to the coupling of the resonance to the compound nuclear states. In the ground state configuration, the spreading width arises from quantal fluctuations in the nuclear shape around equilibrium. At higher temperatures, the probability for the nucleus to acquire different shapes becomes finite. In the adiabatic picture, the time scale of coupling of the resonance to the nuclear shape is long compared to the damping time of the resonance. The nucleus thus samples all possible shapes in the deformation plane, and the measured width is a weighted average of the widths of the resonance built on

all possible shapes.

Ormand *et al.* have performed such adiabatic calculations for the coupling of the GDR to the nuclear free energy surface at finite temperatures [7]. The results of their calculations for ^{208}Pb and ^{120}Sn are shown in figure 2 in comparison to the measured resonance widths.

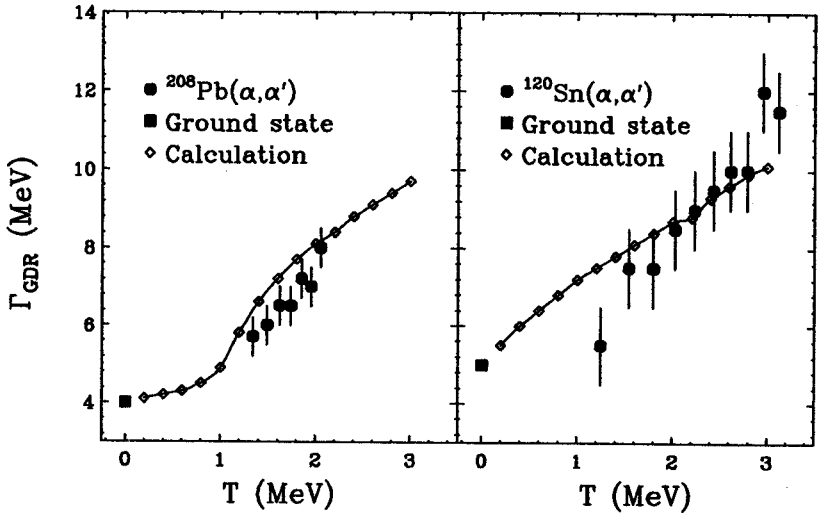

Figure 2: The measured resonance widths (filled circles) are compared to adiabatic coupling calculations (open diamonds and solid line) as a function of nuclear temperature in ^{208}Pb and ^{120}Sn. The filled squares indicate the width of the resonance built on the nuclear ground state.

In ^{208}Pb, the doubly closed shell structure has a strong influence on the resonance properties, and the width does not increase up to a nuclear temperature of ~1 MeV. Beyond this temperature, the nuclear free energy surface broadens with increasing temperature and the GDR width increases systematically. The calculated widths are in good agreement with data over the range of temperatures covered by the measurement. In ^{120}Sn, the shell effects are not prominent, and thus the resonance width starts to increase for non zero values of temperature. This is indicated by the calculated widths displayed in figure 2. The calculation is in good qualitative agreement with the data.

a. Oak Ridge National Laboratory, Oak Ridge, Tennessee.
b. Dept. of Chemistry, Washington University.

References

1. J. J. Gaardhøje, Ann. Rev. Nucl. Part. Sci. 42, 483 (1992).
2. D. R. Chakrabarty *et al.*, Phys. Rev. C 36, 1886 (1987).
3. J. J. Gaardhøje *et al.*, Phys. Rev. Lett. 53, 148 (1984), Phys. Rev. Lett. 56, 1783 (1986).
4. A. Bracco *et al.*, Phys. Rev. Lett. 62, 2080 (1989).
5. D. W. Stracener *et al.*, Nucl. Instr. and Meth. A 294, 485 (1990).
6. S. S. Deitrich and B. L. Berman, Atomic Data and Nuclear Data Tables 38, 199 (1988).
7. W. E. Ormand, private communication.

PARTICLE INSTABILITY OF ^{69}Br

R. Pfaff, D.J. Morrissey, W. Benenson, M. Fauerbach, M. Hellström, C.F. Powell, M. Steiner, B.M. Sherrill, and J.A. Winger[a].

The rapid-proton capture process (rp-process) was first proposed by Wallace and Woosley [1] and showed that heavy isotopes (up to A=100) could be produced in astrophysical processes where high temperatures and densities exist, such as supernova shock waves, novas, and x-ray bursts [2]. The rp-process proceeds via a sequence of proton capture and β^+ decays near and sometimes along the proton drip line. Particle stability and half-lives are important in determining the rate and actual path of the rp-process. Mass models [3] differ on prediction of particle stability along the proton drip line prompting several experiments that looked for the possible termination points of the rp-process [4,5]. The process can be either slowed or terminated when the rp-path must pass through isotopes whose β decay half-life is long relative to the burning time scale of the rp-process. In recent years the odd Z isotopes of ^{65}As and ^{69}Br have been investigated as the most likely termination points.

Evidence for the existence of ^{65}As and ^{69}Br (along with four other new isotopes) was first reported by Mohar *et al.* [5]. A subsequent experiment measured the half-life of several of the isotopes including ^{65}As, however, ^{69}Br was not observed. A recent experiment at GANIL [6] reported five new isotopes (^{60}Ga, ^{64}As, ^{69,70}Kr, and ^{79}Sr) which extended the experimentally observed proton drip line but no events were attributed to ^{69}Br. The latter experiment had a flight path six times longer than the one in Ref. 5, indicating that ^{69}Br could have a very short half life. To explore this possibility a new experiment was performed using the A1200 device [7] at the National Superconducting Cyclotron Laboratory (NSCL) that would be sensitive to very short (~ 100 ns) half-lives.

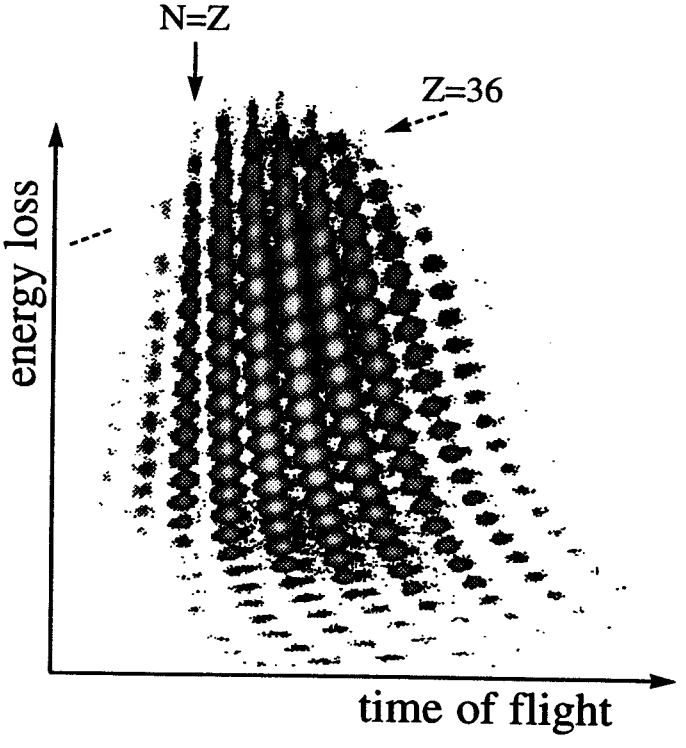

Fig. 1: Energy loss in the first silicon telescope plotted against the TOF enables identification. The N = Z line and the Z = 36 isotope band are indicated by arrows.

A 75 MeV/nucleon ^{78}Kr beam (~ 45 ppA) impinged on a 102 mg/cm^2 ^{58}Ni target in the medium acceptance target position of the A1200. The angular acceptance for fragments was $\Delta\theta$ = 20 mrad and $\Delta\phi$ = 40 mrad centered around 0° with a momentum acceptance of ±1.5%. The magnetic rigidity was varied in overlapping rigidity steps covering the range Bρ = 2.274 to 2.488 Tm. Normalization between the different rigidity settings was done by measuring isotopic yields in the regions of overlapping rigidity. The fragments were stopped in a silicon telescope located at the focal plane of the A1200 or in a second silicon telescope located 7.5 m further downstream from the focal plane. With a very short half life on the order of ~ 100 ns, a reduced isotopic count rate for ^{69}Br would have been observed in the second silicon telescope. The time of flight (TOF) was measured between a 8 mg/cm^2 plastic scintillator at the first dispersive image position and the frontmost detector in the silicon telescopes, with a flight path of 14 m to the first telescope and 21.5 m to the second. The position and angle of the reaction products was measured at both the second dispersive image and the focal plane with pairs of parallel-plate avalanche counters (PPAC's) [8] each separated by 40 cm. The position information at the second dispersive image and NMR measurements of the A1200 dipole fields enabled the momentum of each particle to be determined. Reaction products were implanted into either of the four element silicon telescopes that consisted of two thin ΔE detectors followed by two thick E detectors (100 µm, 75 µm, 500 µm, and 1000 µm). All the silicon detectors had an active area of 300 mm^2. On-line identification was done using the ΔE vs. TOF diagram that is shown in Fig. 1 and shows the excellent energy and time resolution. The absence of ^{69}Br is readily observed. Using the values of ΔE, total kinetic energy, TOF, and magnetic rigidity the mass (A), proton number (Z), and charge (Q) of each particle was determined.

The parallel momentum distribution of each isotope was fitted with a Gaussian function. From the values of the Gaussian centroids the correct setting of the magnetic rigidity for the observation of ^{69}Br was assured. The centroids (in terms of magnetic rigidity) for the isotopes covering Z= 24 to 38 are shown in Fig. 2 where the horizontal dashed lines show the range of magnetic rigidity used for the ^{69}Br setting. The trend

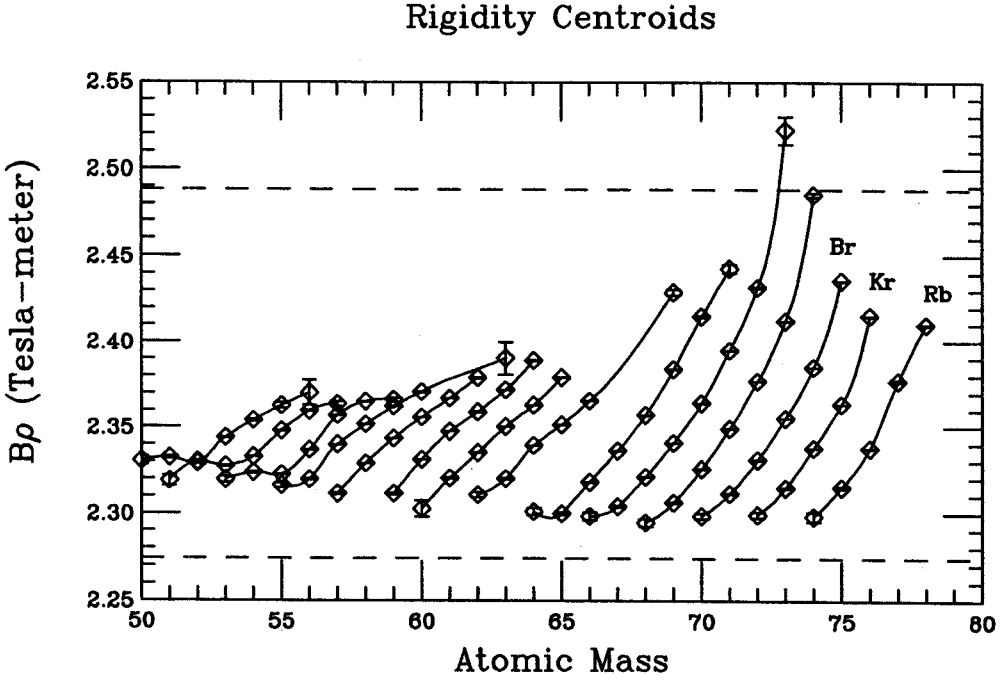

Fig. 2: Momentum distributions were fit with a Gaussian function. The centroids of the Gaussians in terms of magnetic rigidity (Tm) are plotted against the atomic mass for Z = 24 to 37. The projectile-like fragments exhibit the same general trend as is expected from kinematics. The dashed horizontal lines indicate the rigidity region explored during this experiment (2.274 ≤ Bρ ≤ 2.488 Tm).

exhibited by the isotopes, particularly that of bromine, shows that the rigidity settings used for this experiment would have covered the possible range for the observation of ^{69}Br. Shown in Fig. 3 are the measured isotopic cross sections that were determined by integrating the Gaussian fits over momentum space after correcting for the acceptance of the A1200. Using the measured isotopic cross sections it is possible to estimate the number of ^{69}Br events that should have been observed. Assuming an exponential decrease in cross section near the proton drip line (as is predicted by EPAX parameterization [9]) ~ 300 counts of ^{69}Br should have been observed given the number of ^{70}Br events that were identified. Another significant slowing point for the rp-process occurs at ^{73}Rb. The systematics in Fig. 2 show that the magnetic rigidity range covered would have included ^{73}Rb. With EPAX parameterization ~ 75 events of ^{73}Rb should have been observed. This isotope has not been seen in a wide variety of measurements over a number of years.

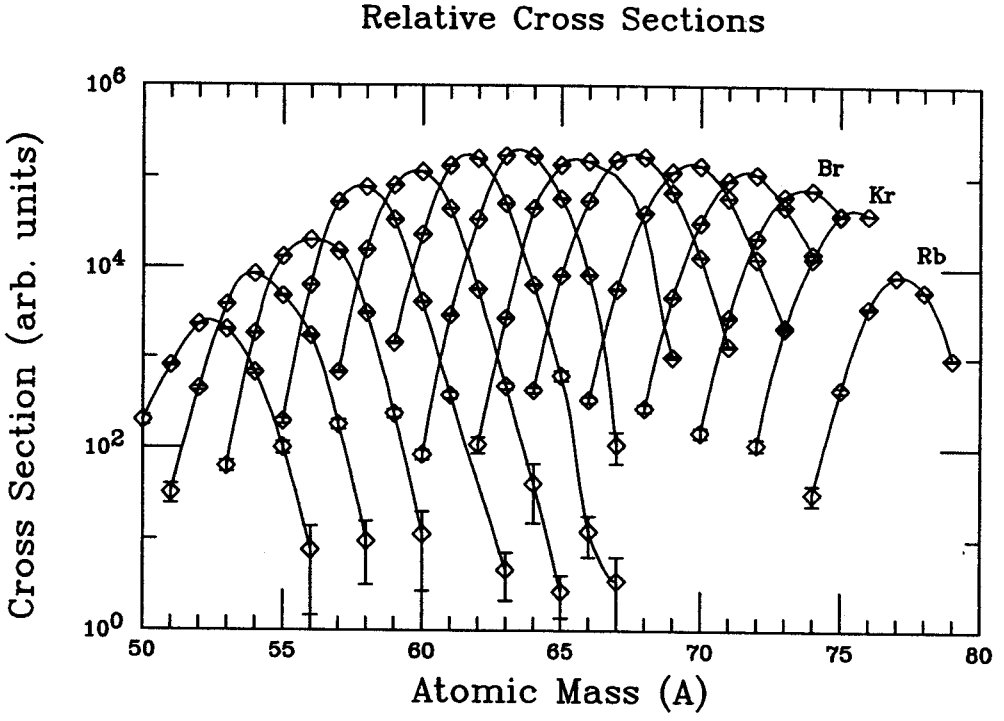

Fig. 3: The relative isotopic cross sections for the elements chromium (Z = 24) through rubidium (Z = 37) are shown here. The cross sections were determined by integrating fitted Gaussian functions over momentum space. The error bars are statistical in nature.

The short flight path (from production target to frontmost silicon telescope was ~ 21 m) combined with the fact that no events were attributed to either ^{69}Br or ^{73}Rb place limits on their half-lives by using the estimated number of events that should have been observed. For ^{69}Br the half-life estimated from the current data is 24 ns or less and the upper limit for ^{73}Rb is 30 ns. Most mass models predict ^{69}Br to be proton unbound but not by a large amount. In the 1993 Atomic Mass Tables [10] the value of S_p = -180 ± 300 keV is found from the listed binding energies of ^{69}Br and ^{68}Se. Using standard barrier penetration calculations, S_p = -180 keV would correspond to a proton emission half-life of ~ 10^6 sec indicating that decay should primarily occur via β-decay which is estimated to be on the order of 100 ms [11]. The recent GANIL experiment [6] limited the ^{69}Br half-life to 100 ns or less which indicates that it is proton unbound by at least 450 keV. The current data places a tighter limit on the ^{69}Br half-life of 24 ns or less that indicates it is proton unbound by at least 550 keV. In the case of ^{73}Rb, the mass models predict this isotope to be proton unbound. The 1993

Atomic Mass Tables give a value of S_p = -590 ± 270 keV that yields a proton emission half-life of ~ 10 ns. The current data shows that ^{73}Rb has a half-life less than 30 ns which indicates that it is proton unbound by at least 500 keV.

The data from the current experiment and the recent GANIL experiment both indicate that ^{69}Br is particle unstable indicating that the rp-path must proceed to higher masses via β-decay of ^{68}Se which has a half-life of 1.6 minutes. The rp-process can continue to higher masses but ^{73}Rb causes another significant slowing point since ^{72}Kr has a 17 second half-life. Five new isotopes were reported in the GANIL experiment that could influence the path of the rp-process and evidence for two of those isotopes was observed during this experiment. Four counts of ^{60}Ga were identified and two events of ^{70}Kr were observed. Measured cross sections for the gallium and krypton isotopes indicate that several events of ^{60}Ga and ^{70}Kr are not unexpected in this experiment. Further investigation should be done to study the properties of the new isotopes in an effort to gain a greater understanding of the exact path of the rp-procss.

a. Mississippi State University, Mississippi State, MS 39762, USA

References

1. R.K. Wallace and S.E. Woosley, Astrophys. J. Suppl. **45**, 389 (1981).
2. L. Van Wormer, J. Görres, C. Iliadis, F.-K. Thielemann, and M. Wiescher, Astrophys. J **432**, 326 (1994).
3. J. Janecke and P.J. Mason, At. Data Nucl. Data Tables **39**, 185 (1988).
4. J.D. Robertson, J.E. Reiff, T.F. Lang, D.M. Moltz, and J. Cerney, Phys. Rev. C **42**, 1922 (1990).
5. M.F. Mohar *et al.*, Phys. Rev. Lett. **66**, 1571 (1991).
6. B. Blank *et al.*, Phys. Rev. Lett. **74**, 4611 (1995).
7. B.M. Sherrill, D.J. Morrissey, J. A. Nolen Jr., and J A. Winger, Nucl. Instrum. Methods B **56**, 1106 (1991).
8. D. Swan, J. Yurkon, and D.J. Morrissey, Nucl. Instrum. Methods A **348**, 314 (1994).
9. K. Sümmerer, W. Brüchle, D.J. Morrissey, M. Schädel, B. Szweryn, and Yang Weifan, Phys. Rev. C **42**, 2546 (1990).
10. G. Audi and A.H. Wapstra, Nucl. Phys. A **565**, 1 (1993).
11. K. Takahashi, M. Yamada, T. Kondoh, At. Data Nucl. Data Tables **12**, 101 (1973).

MULTIPLE SUPERDEFORMED "SEMI–IDENTICAL" ROTATIONAL BANDS IN ^{132}Pr.

C.V. Hampton, R. Aryaeinejad,[a] W.A. Olivier, R. Ronningen, Wm.C. McHarris, and ORNL Nuclear Structure Research Group.[b]

Four superdeformed (SD) rotational bands were observed in a study of high-spin states in odd-odd ^{132}Pr. These bands exhibit remarkably similar transition energies and dynamic moments of inertia. Although the differences in energies and moments are too great to classify them as truly "identical," we have termed them "semi-identical." While somewhat surprising because of so many occurring in one nucleus, their systematics is consistent with more general classes of identical bands in nuclides arising both from the coupling of similar configurations *and* the decoupling of specific particles.

Superdeformation has been observed in several regions of nuclides (for a recent compilation, see Ref. [1]). These areas tend to encompass nuclides that exist with significant static ground-state deformations. One of the regions of recent study is the nuclides around A=130. Several groups have characterized a number of nuclides in this region, observing both highly deformed "regular" bands and SD bands (see, for example [2,3]).

Identical Bands (IB) are defined to be those which differ from a "core" band structure by less than a few percent in terms of either absolute energies of their transitions or dynamic moments of inertia for corresponding transitions. In either case, the rotational structure is apparently dependent on core effects with minimal contributions of the unpaired particles to observable features. The unpaired particle interactions that must exist can be postulated to balance or compensate any core driving effects or be of negligible magnitudes.

SD bands are logical candidates for identical behavior. The uncoupled particles that form the structure are necessarily, by virtue of the high deformation, not strongly interacting with the core structure. It should be common, then, to see more than one band structure which is identical to either a common core structure or another rotational band within these superdeformed nuclides.

Odd-odd nuclides have the advantage of being "one step closer" to both superdeformation and identical behavior in that they start out with two particles that are not paired to core interactions. (The particles in highly deformed nuclides cannot, without creating a driving effect toward a spherical nucleus, occupy a strongly-coupled orbital.) Their existence in highly deformed and necessarily minimally interacting systems provides an origin from which to create these highly deformed (SD) and very minimally interacting (IB) bands.

We investigated the rotational band structure of ^{132}Pr at HRIBF at ORNL. The ^{100}Mo(^{37}Cl,xn) reaction was studied at a beam energy of 160 MeV, determined by a series of test irradiations to maximize production of known levels in the yrast cascade of ^{132}Pr. The target consisted of two self-supporting, isotopically enriched foils which had a total thickness of $\approx$600 μg cm^{-2}. Approximately 3×10^6 coincidences from events with a three–fold or higher multiplicity in the 20 HPGe Compton Suppression Spectrometer γ-ray detector array were recorded on magnetic tape for off-line manipulation and analysis.

All data, calibrated and corrected for Doppler effects, were binned into 2900 x 2900 channel E_γ-E_γ arrays and selected data into 1500 x 1500 channel E_γ(gate)-E_γ-E_γ arrays for subsequent gating and analysis. Spectra of interest were extracted from the 2D arrays and refined (background subtraction and noise reduction) using a Fast Fourier Transform technique [4].

Table 1: Comparison of SD bands in ^{130}La from [3] and ^{132}Pr from present study.

^{132}Pr E_γ	Δ	E_γ	Δ	E_γ	Δ	$E\gamma$	Δ		^{130}La E_γ	Δ
Band 1		Band 2		Band 3		Band 4			1412	
										93
									1319	
										90
									1229	
										81
1186									1148	
	87									75
1099		1083		1075		1025			1073	
	80		73		78		72			75
1019		1010		997		953			998	
	74		83		85		73			77
945		927		912		880			921	
	71		78		91		66			71
874		849		821		814			852	
	88		87		83		84			90
786		762		738		730			762	
	80		77		73		80			
706		685		665		650				
	88		87		76		79			
618		598		589		571				
	83		80		77		82			
535		518		512		489				
	91		100		77		82			
444		418		435		407				

Analysis of the data confirmed the existence of the yrast cascade and extended the high-spin, strongly signature split band reported by Shi *et al.*[5] by five levels. Four new SD bands were also observed, each in coincidence with the 378-keV transition.

Figure 1 shows the 378-keV gated spectrum from the 2D array containing all valid events in the experiment. The transitions of the SD bands are marked with symbols, while other γ rays in ^{132}Pr are labeled with their transition energies. The energies of the transitions of the new SD bands are compiled in Table I. They are compared to the transitions of the SD band in the ^{130}La nucleus, a structure very similar to the ones observed in the ^{132}Pr excitations.

To compare the individual characteristics of the four SD bands in the ^{132}Pr, we have calculated plausible values for the aligned angular momentum. We also calculated the dynamic moments of inertia, and total incremental aligned angular momentum for each band. It is readily seen that the underlying core structure is very similar in each of the four bands. The aligned momentum, plotted in Fig. 2, is nearly indistinguishable for any given transition. The uncertainty of the bandhead spins and specific orbitals couplings involved, causes the large range of plausible initial values.

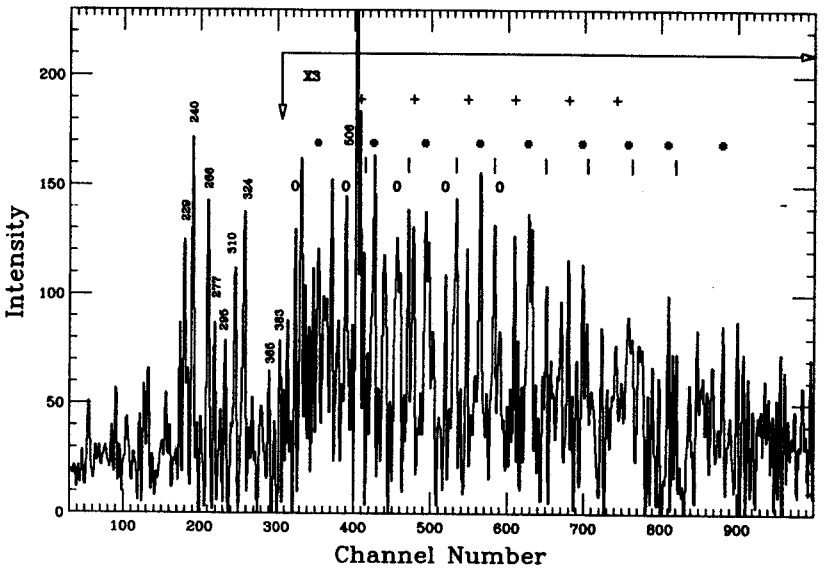

Figure 1: Spectrum gated on 378-keV transition. The four new superdeformed "semi-identical" rotational bands are marked with plotting symbols, other transitions in ^{132}Pr are labeled with transition energies.

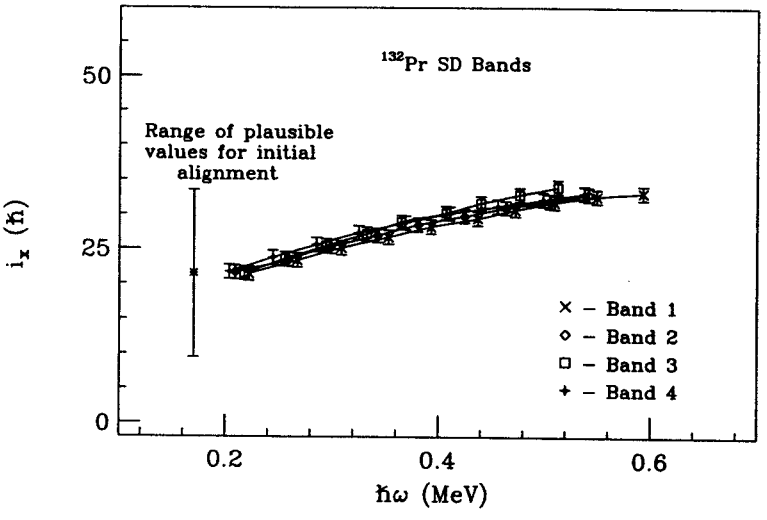

Figure 2: Aligned angular momentum of the SD bands in ^{132}Pr. The large range of plausible values of the initial aligned momentum is due to uncertainties in assigning the bandhead spins and K quantum number for the band.

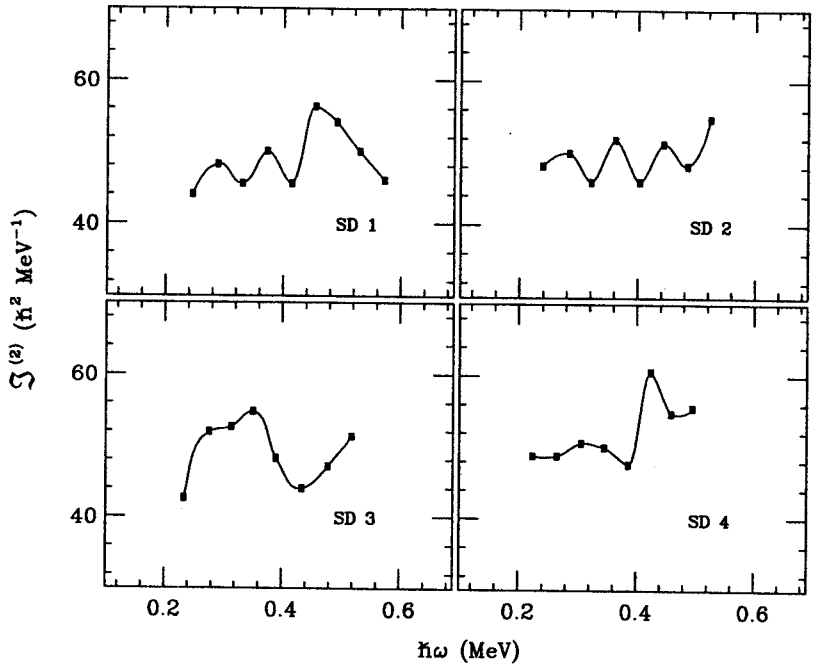

Figure 3: Dynamic moments of inertia for the SD bands in ^{132}Pr.

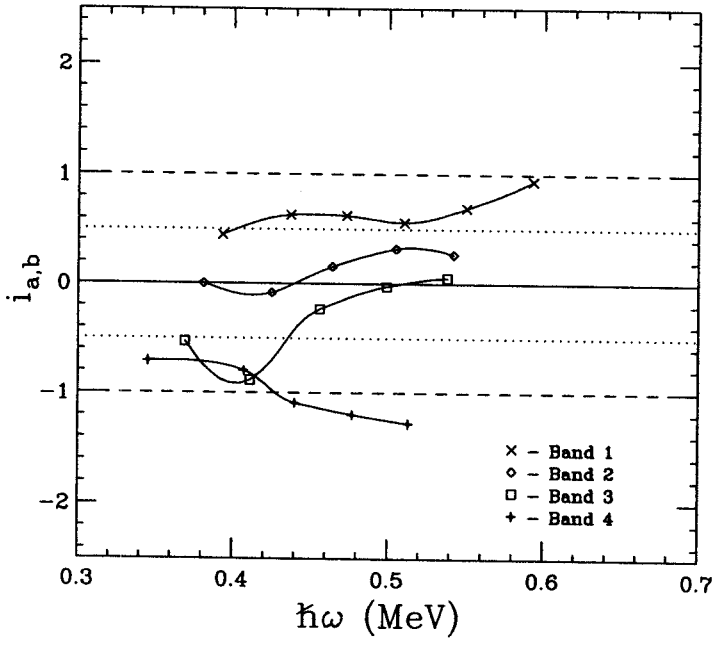

Figure 4: Aligned incremental angular momentum is quantized to integral or half-integral values in "ideal, truly" identical bands. The aligned momenta in the ^{132}Pr SD bands generally clusters about these values.

Ideal SD bands would exhibit level linear plots of dynamic moments of inertia. Figure 3 illustrates the high degree of mixing which must occur among several highly-deformed orbitals in the SD bands in ^{132}Pr.

Stephens *et al.* proposed that the incremental alignment of SD truly "identical" bands is quantized to values of ± 1, ± 0.5, or 0 units of angular momentum [6]. Figure 4 illustrates that these bands do not follow this behavior. Each band does, however, cluster about different, but fairly constant values of alignment. This is still a strong indication of a correlation among the semi-IB-and the SD band in ^{130}La which was used as a reference.

The multiple occurrences of these semi-identical bands is a rare observation. Multiple IB's have been observed in the $A \approx 190$ region, where these cases have demonstrated identical character to a specific "core" rotational band for the immediate region with the IB clustered neighboring nuclides [7]. The behavior observed in ^{132}Pr does not originate in the same manner.

The observation of four semi-identical bands in one nuclide is a stringent test of current thought of identical behavior. While truly identical bands provide an even more exacting arena, these bands illustrate the extent to which "minimal"-interactions of odd (unpaired) particles can effect rotational structures. This behavior is not necessarily limited to superdeformed nuclides. It can also provide insight into behaviors observed in other "identical" structures.

a. EG&G Idaho, Inc., P.O. Box 1625, Idaho Falls, ID 83415
b. Physics Division, Oak Ridge National Laboratory, Oak Ridge, TN 37831

References

1. R.B. Firestone and B. Shigh, *Table of Superdeformed Nuclear Bands and Fission Isomers* LBL Report-35916, 1994.
2. K. Hauschild *et al.* , Phys. Rev. C 50, 707 (1994).
3. E.S. Paul *et al.*, Phys. Rev. C 36, 1853 (1987).
4. C.V. Hampton *et al.*, Nucl. Inst. Meth. A353, 280 (1994).
5. S. Shi *et al.*, Phys. Rev. C 37, 1478 (1988).
6. F.S. Stephens *et al.*, Phys. Rev. Lett. 65, 301 (1990).
7. F. Azaiez *et al.*, Phys. Rev. Lett. 66, 1030 (1991).